GEORGIA INSTITUTE OF TECHNOLOGY
OFFICE OF CONTRACT ADMINISTRATION
SPONSORED PROJECT INITIATION

Date: 10/23/80

Project Title: A Fusion Studies Program

Project No: E-26-656 (NOTE: Continuation of E-26-644)

Project Director: Dr. Weston M. Stacey, Jr.

Sponsor: U.S. Department of Energy; Oak Ridge Operations; Oak Ridge, TN 37830

Agreement Period: From 11/1/79 Until 10/31/80

Type Agreement: Contract No. DE-AS05-78ET52025, Modification No. A002 (formerly Contract No. ET-78-S-05-5683)

Amount: $100,000

Reports Required: Quarterly Technical Progress Reports; Final Report; Publication Preprints; Publication Reprints

Sponsor Contact Person (s):

Technical Matters

C.R. Head
Systems and Applications Studies Branch
Division of Magnetic Fusion Energy
Department of Energy
Washington, D.C. 20545

Contractual Matters
(thru OCA)

Mr. Allen Askew
Research Contracts, Procedures and Reports Branch
Contract Division
Department of Energy
Oak Ridge Operations
P.O. Box E
Oak Ridge, TN 37830
(615) 576-0788

Defense Priority Rating: None

Assigned to: Nuclear Engineering (School/Laboratory)

COPIES TO:

- Project Director
- Division Chief (EES)
- School/Laboratory Director
- Dean/Director–EES
- Accounting Office
- Procurement Office
- Security Coordinator (OCA)
- Reports Coordinator (OCA)
- Library, Technical Reports Section
- EES Information Office
- EES Reports & Procedures
- Project File (OCA)
- Project Code (GTRI)
- Other OCA Property Research Coordinator
- Project Code (OCA)

CA-3 (3/76)

GEORGIA INSTITUTE OF TECHNOLOGY
OFFICE OF CONTRACT ADMINISTRATION

SPONSORED PROJECT TERMINATION

Date: January 15, 1981

Project Title: A Fusion Studies Program

Project No: E-26-656

Project Director: Dr. W. M. Stacey, Jr.

Sponsor: U.S. Department of Energy; Oak Ridge Operations; Oak Ridge, TN 37830

Effective Termination Date: 10/31/80

Clearance of Accounting Charges: - - - - -

Grant/Contract Closeout Actions Remaining:

_ Final Invoice and Closing Documents
_ Final Fiscal Report
_ Final Report of Inventions
_ Govt. Property Inventory & Related Certificate
_ Classified Material Certificate
X Other Certified Statement of Costs

NOTE: Continued by E-26-670

Assigned to: Nuclear Engineering (School/Laboratory)

COPIES TO:

Project Director
Division Chief (EES)
School/Laboratory Director
Dean/Director—EES
Accounting Office
Procurement Office
Security Coordinator (OCA)
✓ Reports Coordinator (OCA)
Library, Technical Reports Section
EES Information Office
Project File (OCA)
Project Code (GTRI)
Other Mr. C. E. Smith

CA—4 (1/79)

Annual Report

November 1, 1979 - October 31, 1980

A FUSION STUDIES PROGRAM

Prepared for the U.S. Department of Energy
under Contract No. DE-AS05-78ET52025

W. M. Stacey, Jr.
Project Coordinator
School of Nuclear Engineering
Georgia Institute of Technology
Atlanta, GA 30332

A FUSION STUDIES PROGRAM

I. INTRODUCTION

Activities in three different areas of tokamak plasma systems analysis were carried out within the Georgia Tech Fusion Studies Program during the period November 1, 1979 through October 31, 1980. These areas are bundle divertor studies, burn control studies and flow reversal studies.

II. BUNDLE DIVERTOR STUDIES

The magnetic and engineering design considerations of a bundle divertor configuration in a tokamak reactor were studied. Codes required to carry out trade-off analyses were implemented. Several divertor configurations were analyzed in an attempt to find an acceptable configuration. At the present time, a configuration which is acceptable from both the field ripple and radiation shielding viewpoints has not yet been found, but progress is being made in this respect. The results of this work will be published in a Georgia Tech Fusion Report (GTFR) in the Fall of 1980, and the work will be continued.

Effects of bundle divertor magnetic field and helical magnetic island structure on self-consistent MHD plasma equilibria were analyzed. Preliminary results indicate that the magnetic islands and ergodic regions produced by the local field perturbations of a bundle divertor can alter the current profile and saturated tearing modes (observed as Mirnov oscillations) in tokamak plasmas. Several computer codes have been developed in the course of this work. Results of this work to date are documented in GTFR-15 and GTFR-16, and the work will continue.

III. BURN CONTROL

The formalism for ion heat conduction due to toroidal field ripple via ripple trapping, banana drift and ripple-plateau effects has been put on a basis that is consistent and computationally tractable. A computer code package incorporating this formalism and a proper averaging over poloidal flux surfaces is being developed. This code and a GTFR report documenting it will be completed in the Fall of 1980.

IV. FLOW REVERSAL

Although not supported by this contract, relevant work on the extension of the Stacey-Sigmar theory (Nuclear Fusion 19, 1665 (1979)) for impurity flow reversal by neutral beam injection to include temperature gradient and heat flux effects was also carried out at Georgia Tech. The extended theory will be published in the Fall of 1980 as a M.S. thesis and in a GTFR report, and the work will be continued under this contract.

ATTACHMENT 1

GTFR-15

EFFECT OF A LOCALIZED MAGNETIC PERTURBATION ON MAGNETIC ISLANDS IN A CYLINDRICAL PLASMA

Glenn Bateman
R. N. Morris

School of Nuclear Engineering
Georgia Institute of Technology
Atlanta, GA 30332

May 1980

NOTICE

ABSTRACT

A self-consistent plasma equilibrium model is developed to study the width of ergodic regions and magnetic islands in a periodic cylindrical plasma under the influence of a localized magnetic perturbation, such as that produced by a bundle divertor or ripple coil set. It is found that localized perturbations tend to produce poloidally symmetric annular ergodic regions and poloidally elongated magnetic islands rather than simple magnetic islands. Our plasma model takes into account the flattening of the current profile across each annular ergodic region and the concommitant steepening of the current profile between ergodic regions. Using current profiles inferred from experimental data, saturated tearing mode amplitudes are computed and found to agree with the experimentally observed Mirnov oscillation amplitudes. As the applied magnetic perturbation is turned on and increased, it is observed that the steepened current profile and resulting enhancement of tearing modes produces wider ergodic regions than would be expected from the vacuum magnetic perturbation alone.

INTRODUCTION

Non-axisymmetric magnetic perturbations in tokamaks are produced by many sources including bundle divertors [1-6], ripple coils [7], helical coils such as those used on PULSATOR [8-9], discrete toroidal field coils [10] as well as tearing modes [11-14] and other naturally occuring instabilities [15-16]. As a direct effect, these magnetic perturbations produce varying amounts of field strength ripple, magnetic islands, ergodic regions, and distortion of the plasma shape. These changes in the magnetic field, in turn, may enhance particle loss (particularly fast particles or trapped particles), may degrade energy confinement (particularly through electrons), and may alter the evolution of plasma instabilities (by changing the plasma profile and producing a disruptive instability, for example). It is particularly important to understand these effects when a deliberate attempt is made to impose a large non-axisymmetric perturbation on a tokamak plasma, as in the case of a bundle divertor, in order to optimize or minimize the effect of the perturbation.

This paper is concerned with the effect produced by the localized magnetic perturbation from a bundle divertor on ergodic regions and magnetic islands within the plasma. While previous studies [1,4] have used a non-self-consistent model in which the vacuum field from the bundle divertor is added to the equilibrium plasma magnetic field, the present study develops a more self-consistent equilibrium model to account for the response of the plasma to the bundle divertor field. This model includes the effect of image currents within the plasma, the effect of naturally occurring magnetic islands due to tearing modes, and

steepening of the current profile as the widths of the magnetic islands or regions of ergodicity are increased by the bundle divertor perturbation. The basic equilibrium model is applied to a cylindrical plasma with periodic end conditions, perturbed by a simple bundle divertor, in the present study.

Some results from field line following using a vacuum magnetic perturbation are presented in section 1, before the self-consistent equilibrium model is developed in section 2, and applied in section 3.

1. OBSERVATIONS FROM A FIELD LINE FOLLOWING CODE

Some observations based on results from a field line following computer code, similar to those reported in Refs. [17-19], will be reported here.

The field line following code integrates the equations

$$\frac{dr(z)}{dz} = \frac{B_r(r,\theta,z)}{B_z(r,\theta,z)} \tag{1}$$

$$\frac{d\theta(z)}{dz} = \frac{B_\theta(r,\theta,z)}{rB_z(r,\theta,z)} \tag{2}$$

given the magnetic field components (B_r, B_θ, B_z) in a periodic cylinder. The location of a given field line (r,θ) in a cross-section of the plasma is plotted as a point after each successive integration along the periodicity length $2\pi R$. Typically 500 points (corresponding to 500 transits) are plotted for a representative field line in order to exhibit magnetic islands or ergodic regions. After trying a number of differential equation solvers, it was found that the Bulirsch-Stoer

extrapolation method used in the IMSL [20] subroutine DREBS was best for the high accuracy needed in this problem. In some cases, a relative error as small as 10^{-10} was needed for good convergence, particularly for very localized magnetic field perturbations. The machine epsilon (the smallest number that can be distinguished from unity) is about 3×10^{-15} on our CYBER 70 computer.

Given a single helical perturbation with radial magnetic field

$$B_r = B_{r1}(r)\cos(m\theta - kz) \quad , \tag{3}$$

where $k = n/R$, a simple analytic estimate for the width of a magnetic island is [14]

$$W \simeq 4r\left(\left|\frac{B_{r1}}{mB_\theta}\ \frac{q}{rq'}\right|\right)^{1/2} \quad , \tag{4}$$

where $q(r) = rB_z/RB_\theta$ and $r = r_s$ is the radius of the mode rational surface on which $q(r) = m/n$. In an effort to check the validity of Eq. (4), the field line following code was used with the vacuum magnetic field from current flowing in a wire along the axis of the cylinder (which yields a high shear magnetic field) and B_{r1} proportional to r. It was found that the magnetic island width is a linear function of the square root of B_{r1} which exceeds the estimate of Eq. (4) by only 2% when the width is two tenths of the minor radius and by only 4% when $W/a \simeq .3$. Hence Eq. (4) provides a remarkably good estimate of the magnetic island width even for large islands.

When two helical harmonics with the same mode rational surface are considered, as for example $m/n = 2/1$ and $4/2$, we find that the

resulting magnetic island width can be determined from Eq. (4) by adding together the B_{r1}/m for each individual harmonic. In other words, the squares of the island widths are additive. The structure of the islands make a continuous transition from m = 2 to m = 4.

When two incommensurate harmonics with overlapping magnetic islands are considered, as for example m/n = 2/1 with width W = .14 and m/n = 7/4 with W = .092, we also find that the squares of the individual widths are additive, so that Eq. (4) can be used if B_{r1}/m are added together from each harmonic. However, the magnetic islands do not deform continuously as in the last case. With even small amounts (10%) of the 7/4 helical perturbation, the x-points of the 2/1 magnetic islands become fuzzy with what appears to be ergodic behavior [21]. When the amplitudes of the perturbations become comparable, the distinct islands give way to a lumpy annular region of apparantly ergodic magnetic field. This persists until B_{r1}/m for the 2/1 perturbation is substantially smaller (much less than 10%) of B_{r1}/m for the 7/4 perturbation. The presence of many incommensurate helical magnetic field perturbations simultaneously can be expected to make the annular ergodic regions more cylindrically symmetric -- less bumpy -- which can be used to simplify our model for the transport-induced current profile, as described in section 2.

The perturbations just considered are sums of helical perturbations, each with $\cos(m\theta - kz)$ dependence. Now consider a perturbation which is localized within a sector $-\theta_m < \theta < \theta_m$, $-z_m < z < z_m$,

$$B^1_r = B_{r1} r\theta(\theta_m^2 - \theta^2)(z_m^2 - z^2)^2$$

$$B^1_\theta = \frac{1}{2} B_{r1} r(\theta_m^2 - \theta^2)^2(z_m^2 - z^2)^2$$

$$B^1_z = 0 \quad ,$$

and identically zero everywhere else, together with a plasma equilibrium field consistent with the current profile

$$J_z(r) = J_{z0}(1 - r^2)^2 \text{ for } 0 < r < 1 \quad ,$$

adjusted so that $1 < q(r) < 3$ within the plasma given $R = 3$. This perturbation has smooth first derivatives and satisfies $\nabla \cdot \vec{B}^1 = 0$. The radial component reverses sign at $\theta = 0$ as illustrated in Fig. 2.

The effect of this perturbation on magnetic islands depends on the sign of the radial perturbation relative to the helicity of the equilibrium field, as illustrated for an m/n = 2/1 island in Figs. 2a and 2b. For the orientation shown in Fig. 2a, field lines just off the q = 2 mode rational surface that drift into the perturbation sector are pushed through the rational surface and drift back out in the opposite direction to form a poloidally elongated magnetic island with x-points at $\theta = 0°$ and $\theta = 180°$ (the nature of the mapping at the q = 2 surface forces the top to bottom reflection symmetry even though the perturbation is localized at only the top in Fig. 2.). For the orientation shown in Fig. 2b, field lines in the neighborhood of $\theta = 0$ (and $\theta = 180°$ by reflection) near the q = 2 surface form small magnetic islands with O-points at $\theta = 0°$ and 180°. Field lines exactly on the q = 2 surface outside of the perturbation sector are left completely unperturbed (e.g. the isolated dots in Fig. 2b). Hence, a localized magnetic

perturbation, similar to that produced by the horizontal legs of a bundle divertor or ripple coil, will produce poloidally elongated magnetic islands as well as smaller structures.

Figs. 2a and 2b were produced by following a selection of field lines which were inside magnetic islands. Field lines outside magnetic islands are characterized by a considerable amount of ergodicity, particularly as the localized perturbation amplitude is increased, as shown in Fig. 3. The annular ergodic regions become smoother -- more cylindrically symmetric -- as the perturbation is made more localized. This is consistent with the fact that more localized perturbations contain a broader spectrum of helical harmonics which, in turn, produce more overlap among magnetic islands. Note that all the radial drift of the field lines shown in Fig. 3 occurs within the localized sector $|\theta| < 0.25$ radians and $|z| < 1$. It was found necessary to integrate with a relative error as low as 10^{-10} for these computations.

2. PERTURBED EQUILIBRIUM

Computational studies of the ergodic regions and magnetic islands resulting from bundle divertors or similar localized magnetic perturbations have generally used a non-self-consistent model in which the vacuum magnetic perturbation from the bundle divertor coil is added to the unperturbed plasma equilibrium magnetic field, as illustrated in the previous section of this paper. It is the purpose of this section to develop elements of a self-consistent model in which image currents and deformation of the current channel within the plasma may have an effect on the width of those ergodic regions and magnetic islands that are driven by the externally applied perturbation, as well as those which occur naturally due to tearing modes. This work is an extension of some

methods used recently by Carreras et al. [13] to predict saturated magnetic island widths (and Mirnov oscillation amplitudes) due to tearing modes and externally applied helical drivers.

It is useful to split off and consider separately the most prominant of those helical harmonies of the magnetic perturbation

$$\mathrm{Re}\left[B_1(r)\exp\, i(m\theta - kz)\right]$$

with resonances within the plasma, $nq(r) - m = 0$, where $k = n/R$, m and n are the poloidal and longitudinal mode numbers, $q = rB_z/RB$, and $2\pi R$ is the periodicity length of the cylindrical plasma being considered. The rest of the magnetic perturbation can be treated as a vacuum magnetic field, relatively unaffected by image currents within the plasma or other self-consistent effects. For example, perturbed plasma currents are not expected to significantly alter the magnetic field ripple or that part of the magnetic field in the bundle divertor chamber outside the main body of the plasma.

In steady state, Maxwell's equations $\nabla\cdot\vec{B} = 0$ and $\mu_o\vec{J} = \nabla \times \vec{B}$ imply, for each helical harmonic,

$$iB_{\theta 1} = \left[-m(rB_{r1})' + kr^2\mu_o J_{r1}\right]/(m^2 + k^2r^2) \tag{5}$$

$$iB_{z1} = \left[kr(rB_{r1})' + mr\mu_o J_{r1}\right]/(m^2+k^2r^2) \tag{6}$$

$$\left[r(rB_{r1})'/(m^2 + k^2r^2)\right]' - B_{r1} \tag{7}$$

$$= r\left[\frac{2mkr\mu_o J_{r1}}{m^2 + k^2r^2} - kri\mu_o J_{\theta 1} - mi\mu_o J_{z1}\right]/(m^2 + k^2r^2)$$

Eq. (7) is used to determine the contribution from any given configuration of coil currents to the particular solution of a helical harmonic radial magnetic field. For example, from a simple pair of bundle divertor coils curved along an arc of constant radius, r_c, the jump in the radial derivative of B_r from $r_c - \varepsilon$ to $r_c + \varepsilon$, in the large aspect ratio limit ($kr \ll m$), is

$$\left[\frac{r(rB_{r1})'}{m^2 + k^2r^2}\right] = \frac{2i\mu_o I}{\pi^2 mn} \sin(m\theta_{max}) \sin^2(kz_{max}) \qquad (8)$$

where I is the current in each coil leg and the coils subtend the arc $-\theta_{max} < \theta < \theta_{max}$ and length $-z_{max} < z < z_{max}$, as illustrated in Fig. 4.

Now consider a force-free perturbed equilibrium

$$\vec{J} \times \vec{B} = 0 \quad . \qquad (9)$$

Most of the current in a tokamak is force-free ($\vec{J}$ is mostly parallel to $\vec{B}$) even when $\beta(\equiv 2\mu_o p/B^2)$ is several percent. The parallel component of the plasma current contributes most to shear and magnetic structure, particularly near mode rational surfaces. Ergodic regions cannot support a steady state pressure gradient in any event. This force-free equilibrium assumption can be relaxed in future work if need be. Note that the force-free equilibrium Eq. (9) together with $\nabla\cdot\vec{B} = 0$ implies that J/B is uniform along field lines.

If Eq. (9) is linearized for a helical harmonic perturbation about a cylindrically symmetric equilibrium ($B_{\theta 0}(r)$, $B_{z0}(r)$) and Eq. (5) and (6) are used to eliminate $B_{\theta 1}$ and B_{z1}, the equation for the radial magnetic perturbation is

$$(krB_{z0} - mB_{\theta 0}) \left\{ \left[r(rB_{r1})'/(m^2 + k^2r^2) \right]' - B_{r1} \right\} \tag{10}$$

$$+ \left\{ r^2 \left[m(rB_{\theta 0})'/r(m^2 + k^2r^2) \right]' + \left[kr^2 B_{\theta 0}(rB_{\theta 0})'/B_{z0}(m^2 + k^2r^2) \right]' \right\} B_{r1} = 0 .$$

and $$J_{r1} = J_{z0}B_{r1}/B_{z0} \quad . \tag{11}$$

In the large aspect ratio limit $kr \ll m$ and $B_{\theta 0} \ll B_{z0}$, Eq. (10) becomes

$$\left[r(rB_{r1}) \right]' - m^2 B_{r1} + mr^2 \left[(rB_{\theta 0})'/r \right]' B_{r1}/(krB_{z0} - mB_{\theta 0}) = 0 \tag{12}$$

Eq. (10) or (12) is to be solved with boundary conditions $B_{r1} \propto r^{m-1}$ at $r = 0$ and $B_{r1} = 0$ at a perfectly conducting wall or at infinity, together with the contributions from applied coil currents (Eq. 7).

Profile with Flat Spots

It is evident that Eqs. (10) and (12) are singular at the radius of the mode rational surface r_s where

$$kr_s B_{z0}(r_s) - mB_{\theta 0}(r_s) = B_{\theta 0}(r_s)(nq(r_s) - m) = 0 \tag{13}$$

However, this singularity is removed if the current profile is flattered in the neighborhood of the mode rational surface -- i.e.,

$$\mu_o J_{z0} = \left[(rB_{\theta 0})'/r \right]' = 0 \quad \text{at} \quad r = r_s \tag{14}$$

in the large aspect ratio limit.

The flattening of the current profile is consistent with the parallel component of Ohm's law

$$\eta \vec{J} \cdot \vec{B} = \vec{E} \cdot \vec{B} = E_z B_{z0} \tag{15}$$

with uniform E_z (in steady state) when there is a poloidally symmetric ergodic region (producing uniform electron temperature and, therefore, uniform parallel resistivity η) in the neighborhood of a mode rational surface. The study of poloidally symmetric ergodic regions is particularly simple since the current profile within each ergodic region is flat (the last term in Eq. (12) is zero) while the current profile between the ergodic regions is determined by the temperature (resistivity) profile together with Eq. (15). With flat spots in $J_{z0}(r)$, Eq. (12) is no longer singular and the linearization of Eq. (9) could be expected to be reasonable. The study of nonlinear effects, other than the flattening of the poloidally symmetric current profile, has led to no further qualitative changes in this model.

For arbitrary ergodic region width around a given mode rational surface, Eq. (12) generally does not have a solution satisfying the boundary conditions. However, a solution can be found by varying the width (and the resulting current profile) until the proper value is found. Effectively the width plays the role of an eigenvalue in Eq. (12). The width of the ergodic region, in turn, is related to the amplitude of the radial magnetic perturbation, by Eq. (4) as described in the last section, which is varied by varying the amplitude of the homogeneous solution of Eq. (12). This is the algorithm we use in this paper to determine the self-consistent solution for a selection of helical harmonics driven by a localized perturbation.

Effectively, this algorithm is an extension of the one used by Carreras et al. [13] to match the experimentally observed Mirnov oscillation amplitude given a model for the experimentally inferred current profiles in ORMAK and T-4. Our algorithm is more flexible in that it

can handle more than one harmonic with the same mode rational surface (e.g. m/n = 2/1, 4/2, 6/3,...) and we can study the simultaneous effect of several ergodic regions on the overall current profile. (Other things remaining equal, the current gradients must become steeper if the flat regions become wider.) Our algorithm is more difficult to implement because the current profile is affected by the widths of the ergodic regions, which are determined iteratively.

Linear Ramp Model

We have implemented the algorithm just described by approximating the current profile by a piecewise linear function of the plasma radius, called a linear ramp model, as illustrated in Fig. 5. Using this approximation, the poloidal magnetic field and longitudinal current density have the form

$$B_\theta(r) = B2(N)r^2 + B1(N)r + BM1(N)/r \tag{16}$$

$$\mu_o J_z(r) \equiv \frac{1}{r}(rB_\theta)' = 3 \cdot B2(N) \cdot r + 2 \cdot B1(N) \tag{17}$$

where B2(N), B1(N) and BM1(N) are coefficients to be determined in each region N = 1,2,... from the center of the plasma to the wall. The current gradient, $\mu_o J_z'(r) = 3\ B2(N)$, is zero in each flat region (N odd) and B2(N) may be prescribed with a different value in each sloped region (N even) or it may be computed, with each iteration of the island widths, by an algorithm designed to hold the edge of the current-carrying region REDGE fixed. In the first region we have BM1(1) = 0 (to avoid singular B_θ at r = 0). B1(1) is prescribed or related to the q-value on axis

$$B1(1) = B_z/Rq(r = 0) \tag{18}$$

and RQ1 is prescribed. The rest of the coefficients are determined by requiring continuity for $B_\theta(r)$ and $\mu_o J_z(r)$ between each region and by computing the position of each mode rational surface

$$q(r) = rB_z/RB_\theta(r) = m/n \quad \text{for} \quad r = RSL(N) \tag{19}$$

self-consistently given the half-width HWL(N) of each flat spot (corresponding to a magnetic island or ergodic region), working from the center to the edge. Hence, the radii of the break points RB(N) which bound the linear segments are determined self-consistently along with the radii of the mode rational surfaces.

Once the equilibrium coefficients and breakpoints are computed for any given set of island widths, the radial magnetic field perturbation equation (Eq. 12) for each mode is integrated out from the center and in from the coils to the mode rational surface, where the amplitude of B_{r1} is made consistent with Eq. (4). The island widths are iterated until solutions with continuous radial derivative are found for all the modes $B_{r1}(N)$ being considered. It was found that the Runge-Kutta-Verner differential equation solver (subroutine DVERK in IMSL [20]) did not converge well when solving Eq. (12) for small island widths. The Adams method in subroutine DGEAR [20], however, works quite well (we normally use a tolerance of 10^{-5}). Newton's method [22] is used together with a set of constraints to force the discontinuity in the radial derivative of each mode (Δ'[11-14]) to zero by iterating on the island widths.

Simple Magnetic Islands

When simple magnetic islands are present, rather than poloidally symmetric ergodic regions, the poloidally averaged current profile looks more like a point of inflection at the mode rational surface [12] rather than a completely flat spot. The gradient of the poloidally averaged current near the mode rational surface must be calculated carefully, since the singularity in Eq. (8) enhances its effect. The corrections needed to study simple magnetic islands as well as the corrections due to the in-out asymmetry of a magnetic island in cylindrical geometry will be calculated in this section.

The helical stream function ψ_* [14], $\nabla\psi_* \times \hat{z} = \vec{B}_*$, is derived by subtracting a zero shear magnetic field for the mode rational surface being considered from the true magnetic field

$$B_{*\theta} = B_\theta(r) - B_\theta(r_s)r/r_s \quad . \tag{20}$$

Using $B_\theta = B1 \cdot r + BM1/r$ and the observed radial magnetic field

$$B_r(r) \simeq B_{r1}(r/r_s)^{-m-1} \sin(m\theta - kz) \tag{21}$$

the helical stream function becomes

$$\begin{aligned} \psi_* &= BM1 \cdot [-\ell n(r/r_s) + \frac{1}{2} r^2/r_s^2] - B_{r1}(r^{-m}/mr_s^{-m} - 1) \cos(m\theta - kz) \\ &= BM1 \cdot \left[\frac{1}{2} + x^2 - \frac{1}{3} x^3 + \ldots\right] - \frac{r_s B_{r1}}{m} (1+x)^{-m} [1 - 2\sin^2 \frac{1}{2} (m\theta - kz)] \end{aligned} \tag{22}$$

where $r \equiv r_s(1 + x)$. The separatrix is given by

$$\psi_*(x,\theta) = \psi_s \equiv \frac{1}{2} BM1 - r_s B_{r1}/m \tag{23}$$

and the half-width by

$$HW = HW_o \sqrt{\frac{(1+x)^{-m}}{\frac{1}{2} - [\ell n(1+x) - x]/x^2}} \tag{24}$$

where $HW_o = W/2$ is given by Eq. (4), and Eq. (24) should be iterated using $x = \pm HW/r_s$ for the outer (+) or inner (-) edge of the island.

Now consider the current profile. Assuming a source of heat near the center of the plasma and neglecting Ohmic heating, the temperature profile and therefore the current profile will be uniform within each magnetic island. The current density will be a function of ψ_*, $J_z = J_z(\psi_*)$, elsewhere. Assuming the current density is a linear function of the radius along a ray passing through the widest part of the island

$$J_z(r) = J_z(r_s) - \left|J'_{zo}\right|(x - HW) \quad \text{along } m\theta - kz = \pi \quad , \tag{25}$$

then the current density outside of the island is

$$J_z(\psi) = J_z(r_s) - \left|J'_{zo}\right|\left[\sqrt{(\psi - \psi_s)/BM1 + HW^2} - HW\right] \tag{26}$$

Now determine the poloidally averaged current density

$$\bar{J}_z \equiv \frac{1}{2\pi} \int_{-\pi}^{+\pi} d(m\theta) J_z(x,\theta) \tag{27}$$

and the coefficient needed for the last term in Eq. (12)

$$\frac{mr^2 \mu_o \bar{J}'_z}{krB_{zo} - mB_{\theta o}} \simeq \frac{r_s^4}{2 \cdot BM1} \frac{\mu_o \bar{J}'_z(r)}{(r - r_s)} \tag{28}$$

After some algebra we find

$$\frac{\mu_o \bar{J}'_z(r)}{r - r_s} = \frac{\mu_o J'_{zo}}{HW} Z(u) \tag{29}$$

where $$Z(u) \equiv \frac{2}{\pi} \int_0^{(\sin^{-1} u,\ \pi/2)} \frac{d\theta}{\sqrt{u^2 + \cos^2\theta}} \tag{30}$$

and $u \equiv (r - r_s)/HW$. The function $Z(u)$, shown in Fig. 6, may be reasonably approximated by

$$Z(u) \approx \begin{cases} 0.63\,u & \text{for } u < 1 \\ \frac{1}{2}\left(1 - \frac{0.17}{u}\right) & \text{for } u > 1 \end{cases} . \tag{31}$$

We have implemented the corrections needed to consider a simple magnetic island [Eqs. (28) - (31)] and radial asymmetry [Eq. (24)] as an option in the linear ramp model. We find that these corrections increase the predicted island width by 30 to 60% and the predicted Mirnov oscillation amplitude by 50 to 80% when only the m/n = 2/1 helical harmonic is considered alone and the profile is adjusted to hold RQ1, r_s, and q_{edge} fixed. The correction for radial asymmetry, taken alone, generally has a smaller effect. If Ohmic heating within the islands were included, the island widths would probably be larger still.

3. RESULTS

Comparison with Experimentally Observed Mirnov Oscillations

In order to check the validity of our model and computer code, and to establish realistic base cases for the subsequent study of the effect of a bundle divertor or similar localized perturbation, an attempt was made to match experimental data provided by M. Murakami and J. L. Dunlap from a series of particularly well documented discharges in ORMAK at ORNL during 1975 [23]. This data consists of Mirnov oscillation amplitudes ($\tilde{B}_\theta/B_\theta$ at the wall) together with toroidal current density profiles inferred from measurements of electron temperature profile and total current. This current profile represents a time average over fluctuations caused by sawtooth oscillations and the

rotating magnetic islands. It was not possible to make direct measurements of current profile or magnetic island widths within the plasma. The same data was used by Carreras et al. [13] as part of their comparison with experiment.

It was observed that the computed Mirnov oscillation amplitudes were quite sensitive to the position of the mode rational surface and to details of the current profile, particularly inside the radius of the mode rational surface. It was not possible to match the experimentally inferred current profiles point by point with our relatively crude linear ramp model. Even after matching the position of the mode rational surface and matching the q-value at the limiter and at the axis, there is still the freedom to choose RQ1, the radius of the first flat spot. The best results were obtained when RQ1 was chosen as large as possible consistent with the experimental data. This choice maximizes the current gradient within the q = 2 surface. In particular, when sawtooth oscillations are present, it was best to choose RQ1 to be the maximum extent of the q = 1 region just after the internal disruption. This is consistent with the observation in PULSATOR [24] that the amplitude of Mirnov oscillations and the probability of major disruption are maximum just after the minor disruption part of the sawtooth oscillation.

The results of this comparison are shown in Fig. 7, where the normalized Mirnov oscillation amplitude, $\tilde{B}_\theta/B_\theta$ for m/n = 2/1 is plotted as a function of the q-value at the limiter. Note, the computed poloidal field perturbation, $\tilde{B}_\theta = iB_{\theta 1}$, is related to the radial field perturbation B_{r1} by Eq. (5), where $J_{r1} = 0$ from the edge of the plasma out. Here, it is assumed here that the wall coincides with the edge of

the plasma. The computed results follow the same trend as the experimental data, but are too low, especially for large q-values. Computed values using the simple magnetic island model come closer to the experimental data than the poloidally symmetric ergodic annulus model. Possibly the inclusion of Ohmic heating within the magnetic islands would bring the results closer.

In a more recent implementation of the linear ramp model, the radius and q-value of the limiter and $q(r = 0)$ are held fixed while the radius of the central uniform-current region is computed. Provision is made for islands to overlap and to eat into the edge of the current profile if necessary. The current profile is computed working from the edge to the center of the plasma with options for either fixed mode rational surfaces or fixed relative current slopes (B2(2n)) which must be adjusted by a computed scale factor to make $B_\theta(r \longrightarrow 0) \longrightarrow 0$. The new algorithm was found to be particularly useful for studying bundle divertors, where the magnetic structure determines the edge of the current profile. The + marks in Fig. 7 show the Mirnov oscillation amplitudes computed using the new alorithm with only the m/n = 2/1 helical harmonic with fixed mode rational surface matching the experimentally inferred radius of the q = 2 surface. In most cases, this procedure gave excellent agreement with experimental observations.

Effect of a Bundle Divertor

An example of the effect of a simple bundle divertor on the width of poloidally symmetric ergodic regions in a cylindrical plasma is described in this section. The bundle divertor being considered here consists of a pair of square-shaped coils curved along an arc of constant radius, illustrated in Fig. 4, whose contribution to the helical

harmonic field is described by Eq. (8). For this particular study, $z_{max} = .8$, $r_{COIL} = 1.2$, $r_{WALL} = 3.$, $r_{COIL} \cdot \theta_{max} \doteq .4$, the plasma radius and longitudinal field are normalized to unity while the aspect ratio was taken to be R = 3.57 (to be consistent with ORMAK data). Significant divertor action is achieved with $\mu_o I/aB_z = .3$. Only the lowest order harmonics with resonances within the plasma will be considered here.

The transition from a simple magnetic island produced by a saturated tearing mode (generally m/n = 2/1) to a poloidally symmetric ergodic region was not studied. From the observations made at the end of section 2, it can be inferred that the contribution from the tearing mode will be reduced by 30 to 60% during this transition. Here, only poloidally symmetric ergodic regions will be considered.

As the current in the bundle divertor is increased, many changes happen simultaneously within the plasma as the ergodic regions grow wider and the current profile changes. Figure 8 shows the effect of the simple bundle divertor on the m/n = 2/1 and 3/1 helical harmonics, holding the positions of the mode rational surfaces fixed corresponding to the experimentally inferred profile with q-limiter = 4.2 and q(0) = 1.0 (second data point from left in Fig. 7). Figure 9 shows the same case with the more realistic assumption of fixed relative current slopes adjusted by a scale factor. The new algorithm, working from the edge to the center was used in both cases, with q-limiter (total plasma current) and q(0) held fixed as the divertor is turned on. The computed half-widths of the ergodic regions are plotted as a function of bundle divertor current in the upper portions of Figs. 8 and 9. For comparison, the dashed curves indicate the half-widths produced by the vacuum magnetic perturbation for the 3/1 and 2/1 modes (they happen to be nearly identical in Fig. 8) using the same poloidal field $\left(B_\theta(r), q(r), q'(r)\right.$

in Eq. (4)) as in the self-consistent calculation. The lower portion of Figs. 8 and 9 show the linear ramp current profiles with the bundle divertor off (solid line) and on (dashed line), with the experimentally inferred current profile (smooth curve, no divertor) shown for comparison.

In Fig. 8, with fixed mode rational surfaces, the self-consistently computed 3/1 half-width is consistently wider than the vacuum field prediction, while the 2/1 half-width drops slightly below the unperturbed value until it becomes comparable with the vacuum half-width, as the bundle divertor current is increased. This behavior can be understood by noting that the current profile between the 2/1 and 3/1 islands becomes steeper as the divertor is turned on, while the profile becomes less steep between the 2/1 island and the center of the plasma. In general, the saturated tearing mode amplitude increases as the current profile becomes steeper on the inner edge or shallower on the outer edge of the magnetic island, and vice versa. Hence the changing current profile has enhanced the 3/1 saturated tearing mode at the expense of the 2/1 mode.

In the more realistic case where the relative slopes of the current profile are fixed, shown in Fig. 9, the 3/1 island width remains nearly the same as that predicted by the vacuum perturbation while the 2/1 width is approximately the sum of the vacuum width and the unperturbed saturated tearing mode width. The islands significantly erode the edge of the current profile and force the central $q = 1$ region (sawtooth oscillation region) to expand in order to accommodate the same total plasma current. It was not possible to obtain convergence as the bundle

divertor current was increased further, since the broader islands and correspondingly steeper current profile greatly enhanced the saturated tearing modes, which made the islands still broader and profile steeper, in a process analogous to the disruptive instability.

4. CONCLUSIONS

Several effects happen simultaneously when a localized magnetic perturbation is applied to a current-carrying plasma. A very localized perturbation tends to produce poloidally symmetric annular ergodic regions and poloidally elongated magnetic islands rather than simple magnetic islands. The poloidally averaged current profile is more completely flattened in each of these annular ergodic regions than it would be with simple magnetic islands. The saturated tearing mode amplitude is smaller with ergodic regions than with simple magnetic islands. The amplitude of saturated tearing modes depends sensitively on details of the current profile, increasing as the current gradient just inside the mode rational surface is increased or as the current gradient just outside the mode rational surface is decreased. As the applied perturbation is increased, the width of the ergodic regions and the current gradient between them increases, which enchances the saturated tearing mode amplitude for at least some of the modes. These changes in current profile and their effect on tearing modes appear to be more important than the direct effect of helical image currents in the plasma.

The most important change being planned in the algorithm is to replace Eq. (4) with a more realistic estimate of the ergodic region width when there are many harmonics with the same mode rational surface.

Equation (4), when used with only the lowest order resonant harmonic, as done in the present study, probably overestimates the ergodic region width since the harmonics of a localized perturbation cancel almost everywhere. Studies done to date with up to 8 helical harmonics with different mode rational surfaces have indicated that higher harmonics ($m \geq 4$) tend to be well approximated by the vacuum perturbation. This should make it easier to determine the true widths of ergodic regions by using a field line following code as in section 1.

Another improvement being considered is to use a transport code to determine the electron temperature profile and therefore obtain a better approximation to the current profile between ergodic regions, rather than relying on the ad hoc procedures used in the present study. Unfortunately, the electron heat conductivity and radiation loss mechanisms have so far been only crudely approximated by empirical models. Given the demonstrated sensitivity to current profile, it is not clear if there would be any advantage to studying these modes in toroidal geometry at this stage.

Acknowledgments

We would like to thank Drs. Masanori Murakami and Julian Dunlap for generously providing detailed experimental data taken on the ORMAK tokamak at Oak Ridge National Laboratory. We would like to dedicate this work to the memory of Dr. B. V. Waddell and to acknowledge the encouragement and suggestions from Drs. B. Carreras, H. R. Hicks, J. A. Rome, J. N. Davidson and W. M. Stacey. This research was supported by the U.S. Department of Energy under contract no. DE-AS05-78ET52025.

Figure Captions

Fig. 1 Magnetic structure near the q = 2 surface produced by two helical perturbations m/n = 2/1 and 7/4 in the cylindrical field of a current filament at r = 0 with aspect ratio 3 and $B_z = 1$. Radial field perturbation amplitudes are noted at the q = 2 surface.

Fig. 2 Cross section of the m/n = 2/1 magnetic island produced by a localized magnetic perturbation confined to the sector $|\theta| < 1$ radian, $|z| < 1$ with amplitude $B_{r1}/B_{z0} = .04$ in (a) and $|\theta| < .5$, $|z| < 1$, $B_{r1}/B_{z0} = -0.32$ in (b).

Fig. 3 Sample of the magnetic structure produced by a localized magnetic perturbation confined to the sector $|\theta| < 0.25$ radians, $|z| < 1$, with amplitude $B_{r1}/B_{z0} = 2.56$.

Fig. 4 Schematic of the simple bundle divertor coil set, used in this paper [Eq. 8], in the cylindrical surface r = constant.

Fig. 5 Schematic of the linear ramp current profile as a function of radius in a cylindrical plasma.

Fig. 6 Function Z(u) defined by Eq. (30).

Fig. 7 Computed m/n = 2/1 Mirnov oscillation amplitudes at the limiter (= wall radius here) compared with experimental data from ORMAK [23]. The x and o points are computed using the best match to the experimentally inferred current profile while the + points are computed just matching the inferred radius of the q = 2 surface.

Fig. 8 Effect of a simple bundle divertor (Fig. 4) on ergodic region half-widths (top) and current profile (bottom) holding the radii of the q = 2 and q = 3 surfaces and $q_{limiter} = 4.2$ fixed. The dashed line at top are the nearly coincident half-widths computed from the vacuum field perturbation. The smooth curve at bottom is the experimentally inferred current profile.

Fig. 9 Effect of a simple bundle divertor on ergodic region half-widths (top) and current profile (bottom) holding the relative slopes of the current profile and $q_{limiter} = 4.2$ fixed.

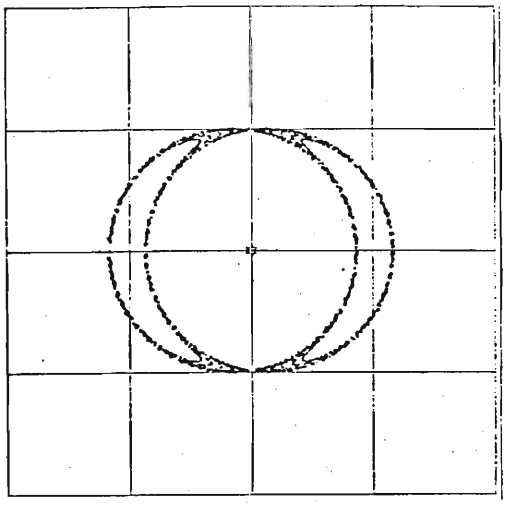

$B_{r21} = .002$
$B_{r74} = .0$

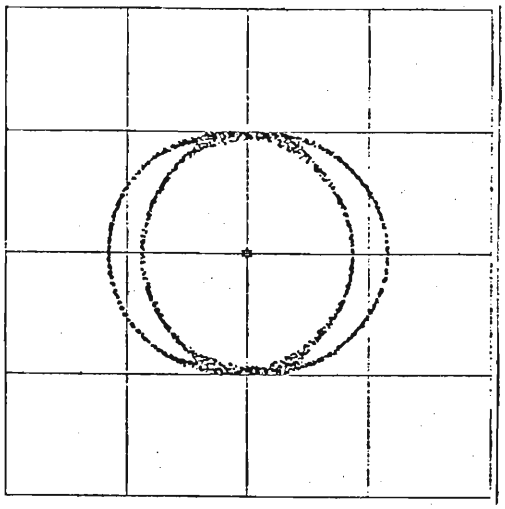

$B_{r21} = .0018$
$B_{r74} = .0002$

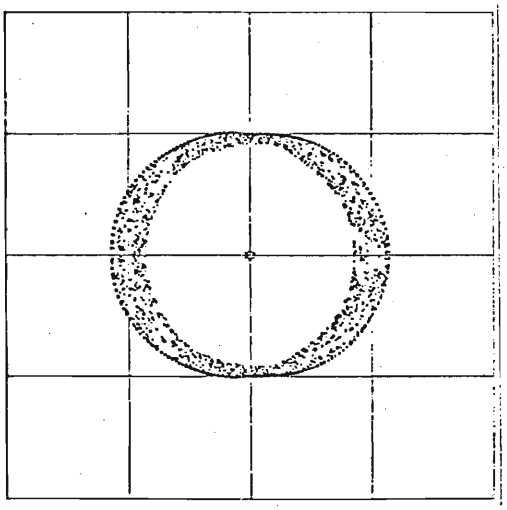

$B_{r21} = .0014$
$B_{r74} = .0006$

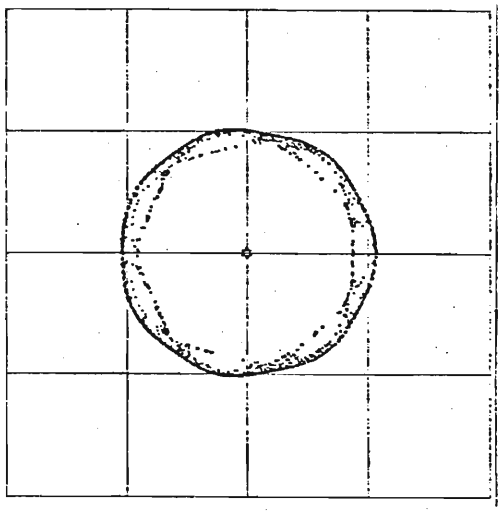

$B_{r21} = .0002$
$B_{r74} = .0018$

FIG. 1.

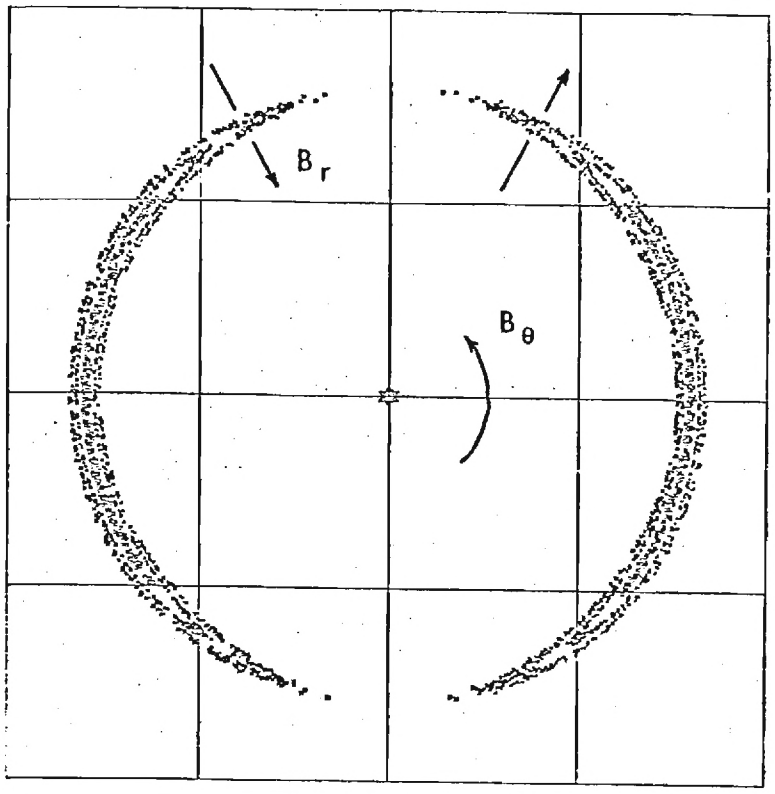

(a)

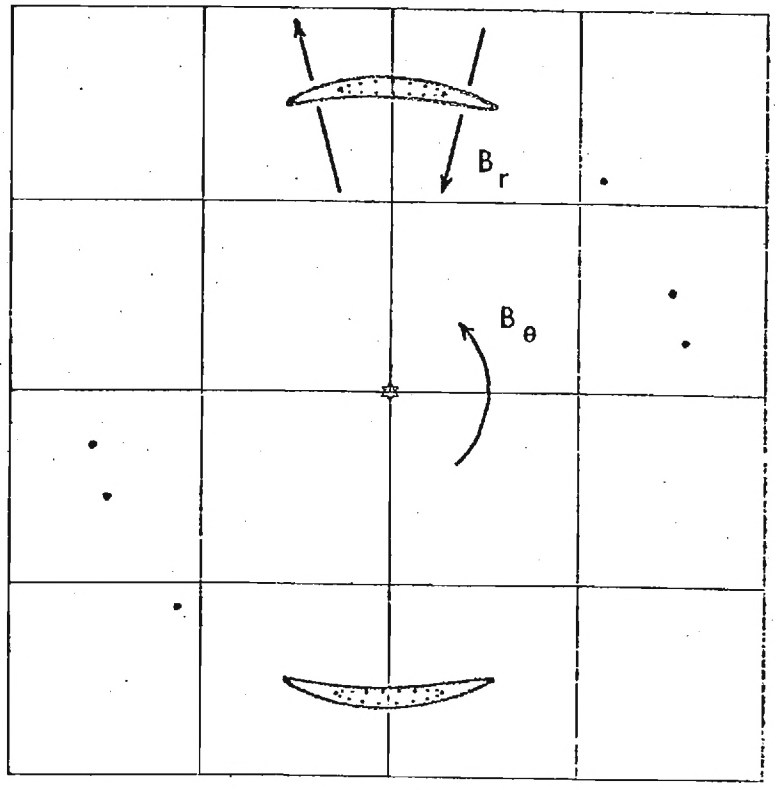

(b)

FIG. 2

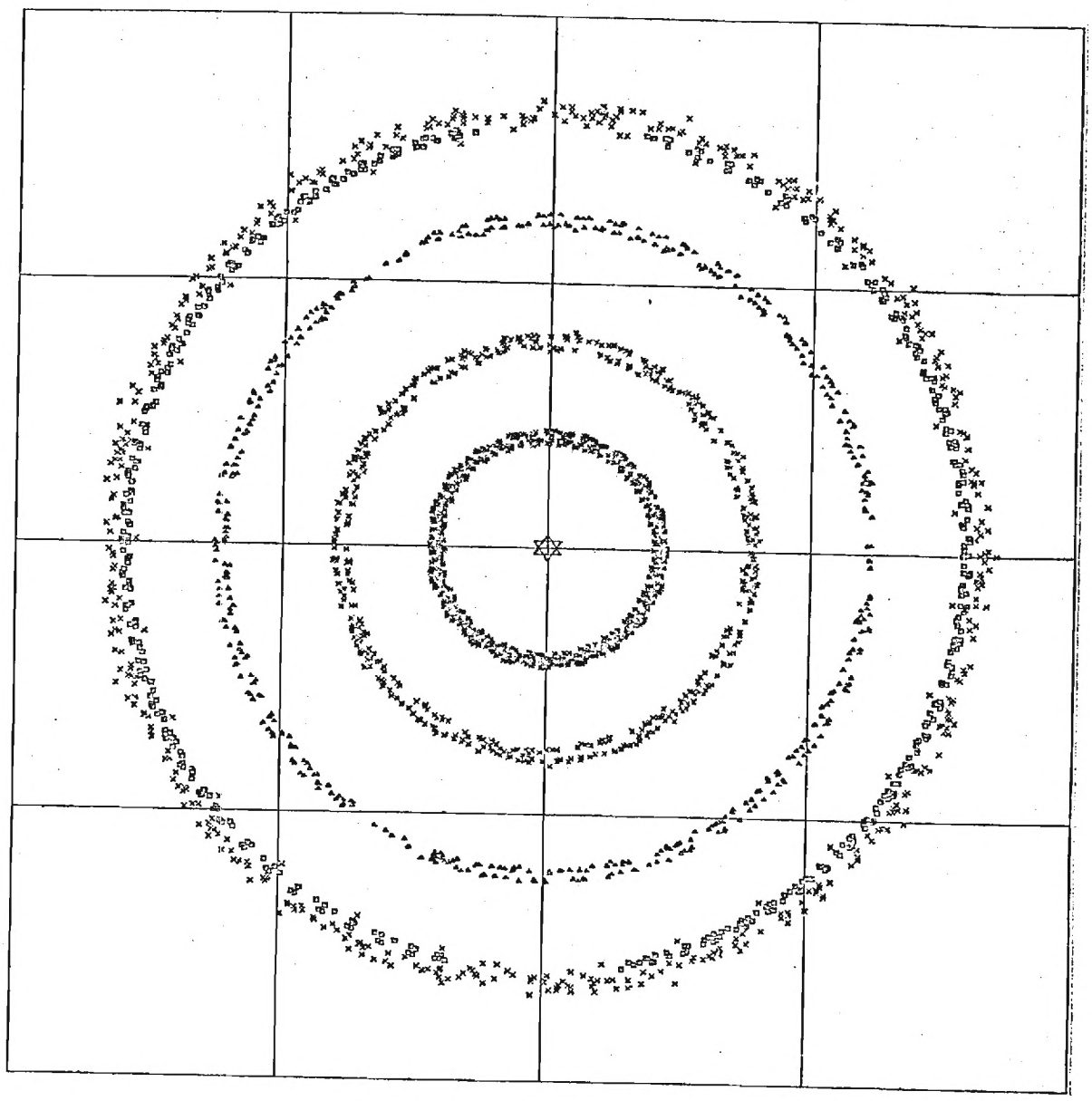

FIG. 3.

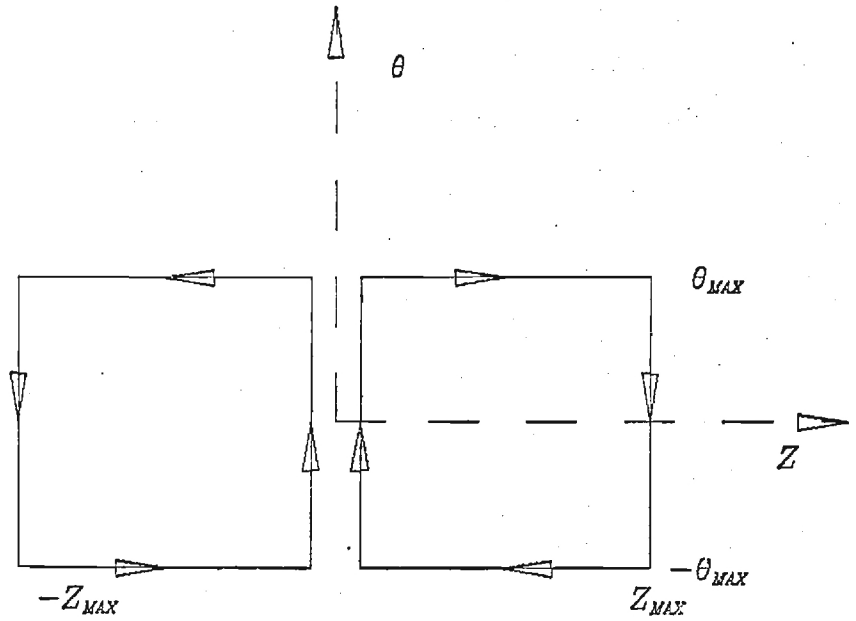

FIG. 4.

FIGURE 5

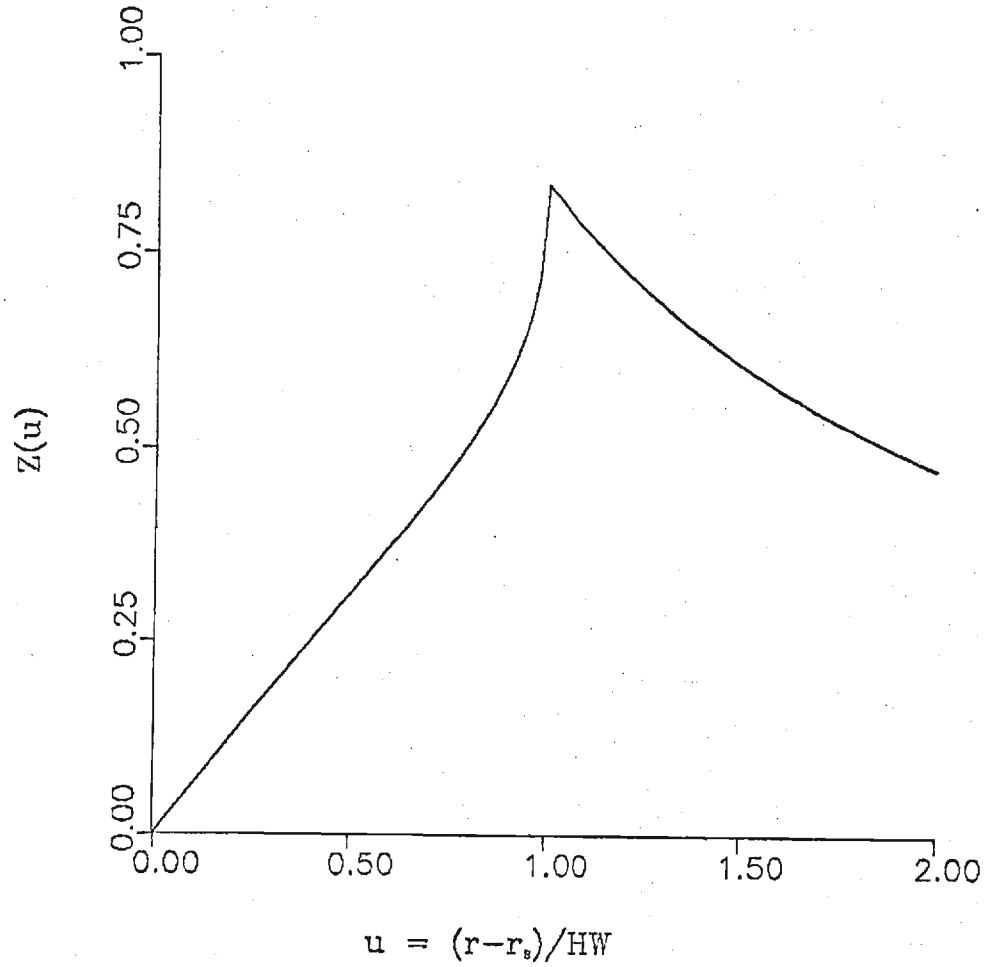

FIG. 6

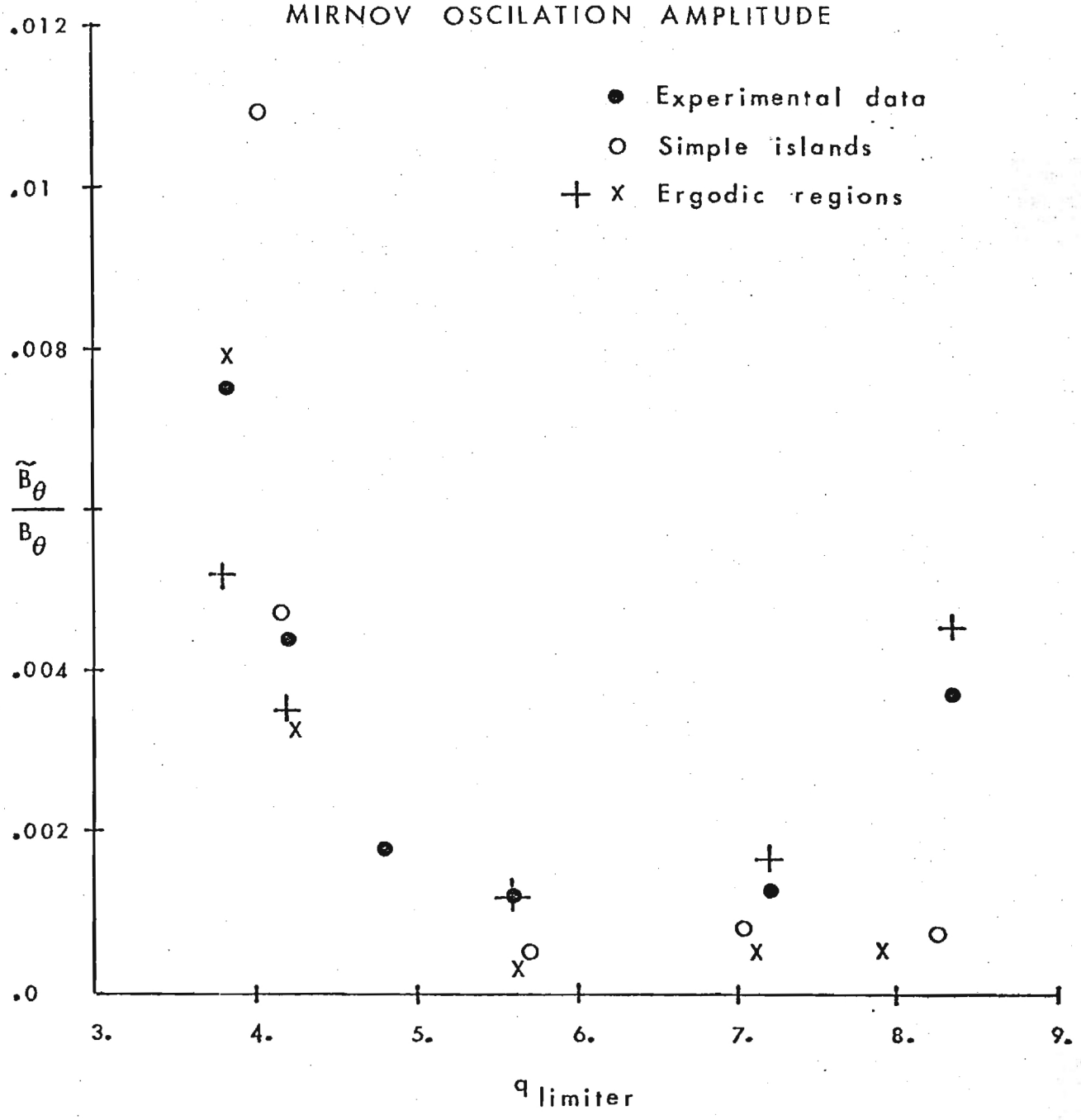
MIRNOV OSCILATION AMPLITUDE
Experimental data
Simple islands
Ergodic regions
.012
.01
.008
.004
.002
.0
$\frac{\tilde{B}_\theta}{B_\theta}$
3.
4.
5.
6.
7.
8.
9.
$q_{limiter}$

FIG 7

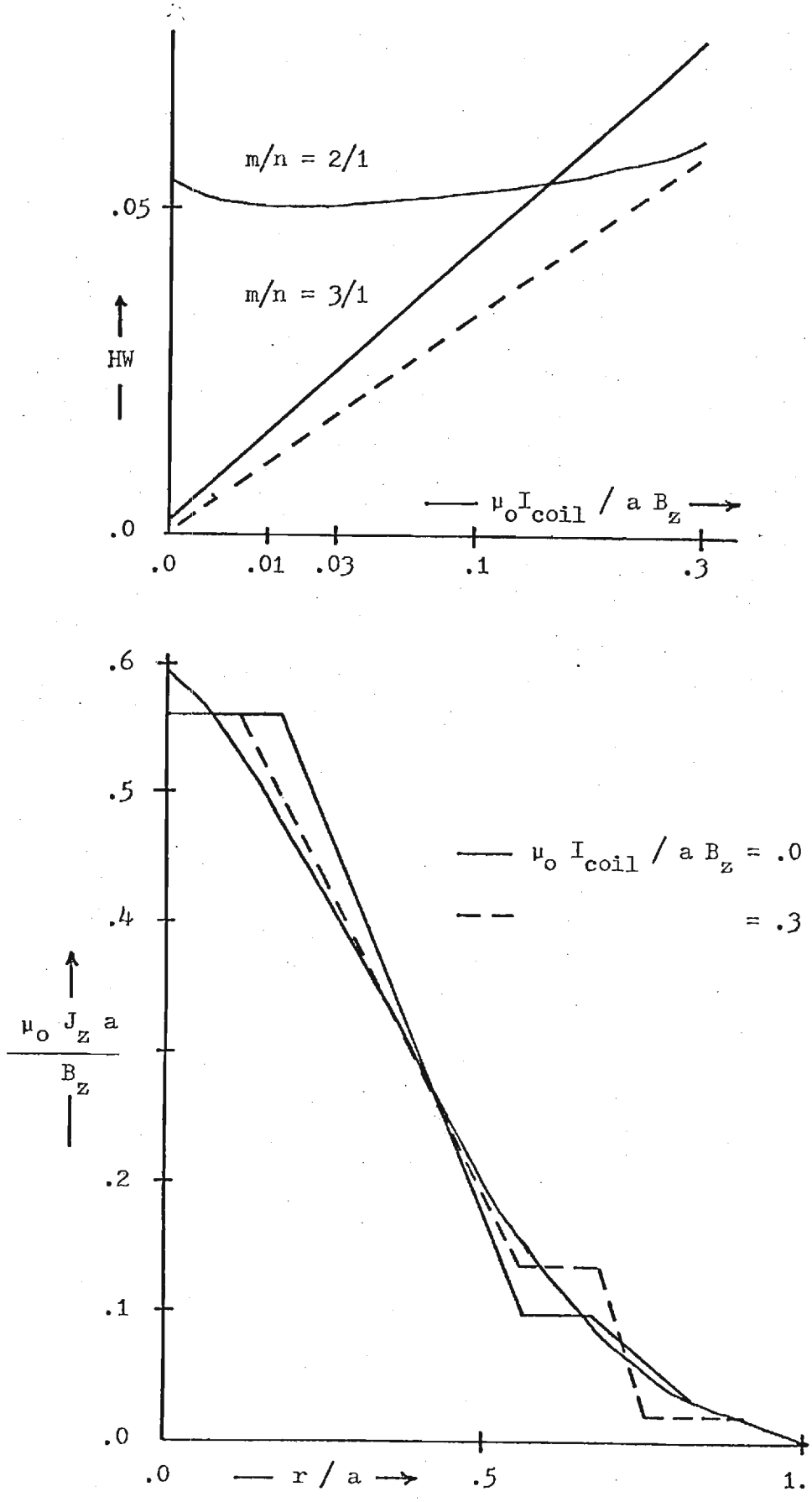
m/n = 2/1
m/n = 3/1
.05
.0
HW
$\mu_o I_{coil} / a B_z$ →
.0
.01
.03
.1
.3
.6
.5
.4
.2
.1
.0
$\mu_o I_{coil} / a B_z$ = .0
= .3
$\mu_o J_z a / B_z$
.0
r / a →
.5
1.

FIG. 8.

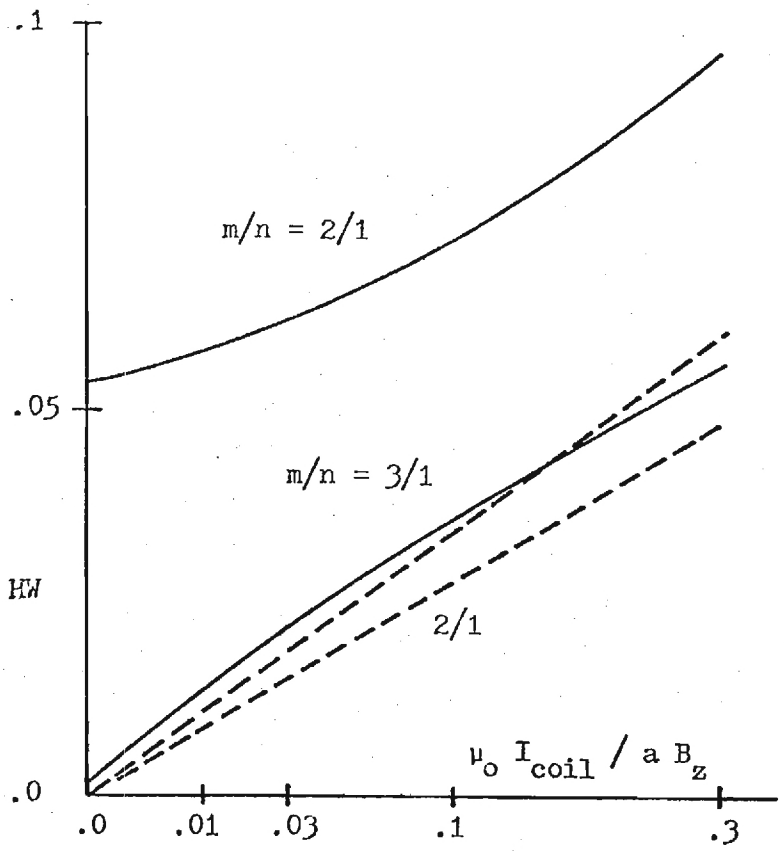
.1
.05
.0
HW
m/n = 2/1
m/n = 3/1
2/1
μo Icoil / a Bz
.0
.01
.03
.1
.3

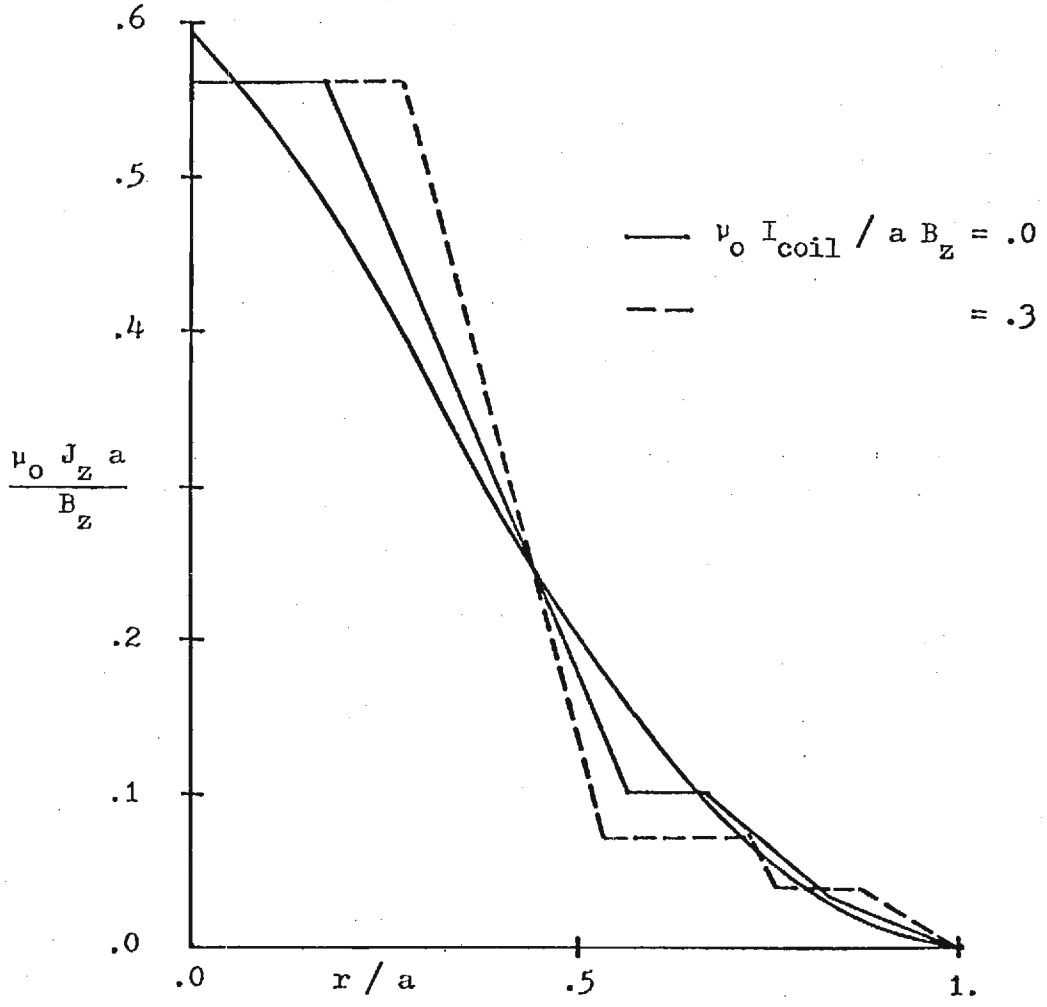
.6
.5
.4
.2
.1
.0
μo Jz a / Bz
μo Icoil / a Bz = .0
= .3
.0
r / a
.5
1.

FIG. 9

REFERENCES

[1] STOTT, P. E., C. M. Wilson and A. Gibson, Nucl. Fusion 17 (1977) 481, Part I, and Nucl. Fusion 18 (1978) 475, Part II.

[2] STOTT, P. E., et al., in Plasma Wall Interaction (Proc. Int. Symp., Julich, 1976), Pergamon Press EUR 5782e, Oxford (1977) 39.

[3] SHEFFIELD J. and R. A. Dory, "The Ripple Bundle Divertor for Tokamaks," ORNL/TM-6220 (1978).

[4] Workshop on Physics and Engineering Problems of Divertors in Tokamak Reactors, (RUTHERFORD, P. H., ed.) Princeton Plasma Physics Laboratory (July 1979).

[5] WELLS, W. M., "ORNL TNS Program: Evaluation of the Bundle Divertor," ORNL/TM-6727 (November 1979).

[6] STACEY, W. M., J. R. Gilleland, G. L. Kulcinski, P. H. Rutherford, et al., "INTOR: The U.S. Contribution to the International Tokamak Reactor Workshop 1979," IAEA (November 1979).

[7] LYON, J. F. and J. A. Rome, Bull. Am. Phys. Soc. 24 (1979) 1034.

[8] KARGER, F., et al., in Plasma Physics and Controlled Nuclear Fusion, IAEA (1975) Vol. 1, 207 and IAEA (1977) Vol. 1, 267.

[9] LACKNER, K. and F. Karger, "Stabilization of Disruptive Instability by Resonant Helical Windings," Ann. Controlled Fusion Theory Conf., San Diego (1977).

[10] GOLDSTON, R. J. and H. H. Towner, Bull. Am. Phys. Soc. 24 (1979) 1045.

[11] RUTHERFORD, P. H., Phys. Fluids 16 (1973) 1903.

[12] WHITE, R. B., D. A. Monticello, M. N. Rosenbluth, B. V. Waddell, Phys. Fluids 20 (1977) 800.

[13] CARRERAS, B, B. V. Waddell and H. R. Hicks, Nucl. Fusion 19 (1979) 1423.

[14] BATEMAN, G., MHD Instabilities, The M.I.T. Press, Cambridge, 1978.

[15] ZWEBEN, S. J., Bull. Am. Phys. Soc. 24 (1979) 1072.

[16] CALLEN, J. D., et al., in Plasma Physics and Controlled Nuclear Fusion Research 1978, IAEA (1979) Vol. 1, 415.

[17] VUILLEMIN M. and C. Gourdon, EUR-CEA-FC-393 (Fontenay-aux-Roses, France, 1967).

[18] CHRISMAN, P., J. Clarke and J. Rome, ORNL/TM-4501 (1974).

[19] FINN, J. M., Nucl. Fusion 15 (1975) 845.

[20] IMSL Library, Edition 7, International Math Science Library.

[21] BERRY M. V., in "Topics in Nonlinear Dynamics," (JORNA, S., ed.), (Am. Inst. Phys., New York, 1978) 16-120.

[22] FORSYTHE, G. E., M. A. Malcolm and C. B. Moler, Computer Methods for Mathematical Computations, Prentice-Hall, New Jersey, 1977.

[23] MURAKAMI, M. and J. L. Dunlap, private communication, 1980; ORNL/TM-5154 (1976) 20.

[24] ENGELHARDT, W., et al., in Plasma Physics and Controlled Nuclear Fusion Research 1978, IAEA (1979) Vol. 1, 123.

ATTACHMENT 2

GTFR-16

DIVERT

A Divertor Magnetic Field Line Following Code

by

R. N. Morris and Glenn Bateman
School of Nuclear Engineering
Georgia Institute of Technology
Atlanta, GA 30332

May 1980

NOTICE

ABSTRACT

The computer code DIVERT has been written to trace magnetic field lines in the presence of a divertor. Its purpose is to allow a user to estimate the thickness of the plasma scrapeoff region and to provide a visual mapping of the magnetic field lines near the divertor. Included in the code is the capability to provide auxiliary graphics and compute the field ripple. The code can handle a divertor made up of any arrangement of straight line coil segments and will provide a graph of the field line configuration or output.

Introduction

The DIVERT computer code will allow a user to plot out the magnetic field line configuration near a bundle divertor. The user submits the major parameters of the tokamak and the line segment construction of the divertor along with the currents. Also included is a capability of drawing auxiliary lines on the graph. This graphic capability may be used to include various other nearby devices (pumps,magnets,neutral beam injectors,etc.) and so provice a means of determining "fit", since everything is drawn to scale.

The output is a graph of a selection of magnetic field lines, an outline of the torcus, divertor, and any other auxiliary graphics.

Theory

The DIVERT code integrates the following equations for the field lines;

$$\frac{ds}{B} = \frac{dx}{B_x} = \frac{dy}{B_y} = \frac{dz}{B_z}$$

The magnetic field at point $\vec{X}$ from any given straight line coil segment between $\vec{X}_1$ and $\vec{X}_2$ is

$$\vec{B} = \frac{\mu_0 I_{COIL}}{4\pi} \frac{\vec{X}_3 \times \vec{X}_1}{|\vec{X}_3 \times \vec{X}_1|^2} \left[\frac{\vec{X}_3 \cdot \vec{X}_1}{|X_1|} - \frac{\vec{X}_3 \cdot \vec{X}_2}{|X_2|} \right]$$

where $\vec{X}_1 = \vec{x}_1 - \vec{x}$ $\quad \vec{X}_2 = \vec{x}_2 - \vec{x}$ $\quad \vec{X}_3 = \vec{x}_2 - \vec{x}_1$

and ICOIL is the current from $\vec{x}_1$ to $\vec{x}_2$

See figure 1. This is added to the toroidal magnetic field

$$\vec{B}_T = \frac{BZA}{R}$$

The poloidal magnetic field is not incorporated at present, but it is a simple matter to add it in MAGFLD.

The computer program uses the differential equation solving subroutine DREBS from the computer library IMSLIB. Several other subroutines for solving the differential equations were tried, but DREBS provided the higher accuracy results for this type of problem. Other types of library subroutines are used in this computer code: The plotting routines from CALCOMP and the author's own library, RNMLIB, are used throughout the code. Please note that the submit file DSUB and some of the particulars of the input are local to the Georgia Tech computer

system (as of April 1980).

Input data

The input consists of three namelists and several lines of alpha numeric data. See table 1 for a list of the major Fortran variables.

The first portion of the input is the namelist PRAM. PRAM contains,

RADIUS

ASPECT

SCALE

CURRENT

The second namelist to be entered is IN. IN contains,

NLINE

XS(20)

YS(20)

NCOIL

V(7,20)

TOL

BPA

BZA

The only item to note is that the V7's should contain only the relative current so that scaling the current can be done by means of CURRENT. TOL is the integrator tolerance and can be varied for accuracy or different runs. For first "roughing" runs, it should be about 1.E-3 to 1.E-4.

The third namelist is GRAPH. G is an array which contains the coordinates of points to be plotted on the output graph. There are two graphing commands 1.E3 and 1.E4. G(n,1) is the x coordinate and G(n,2) is the z coordinate. Normally a line is drawn from G(n-1,1) , G(n-1,2) to G(n,1),G(n,2). If G(n,1) = 1.E3, the pen is lifted for the move from G(n-1,1),G(n-1,2) to G(n+1,1),G(n+1,2). If G(n,1) = 1.E4 the graphing is terminated.

The final input data is the alpha numeric data. The first line is the run number, which is a line of alpha numeric data (20 characters max). The following line is a switch input and must contain either a YES or a NO. If it contains a NO, this is the end of the input data. If it contains a YES, the next three lines can contain any alpha numeric data which will be printed on the output graph. Note that three lines must be filled - pad with blanks if necessary.

This completes the input data.

Results

The following figures (2-4) show the results of several runs with three types of bundle diverters.

Acknowledgement

This work is supported by the U.S. Department of Energy, Contract No. DE-AS05-78ET52025.

TABLE 1

Fortran variables

BR(1)	X Coordinate
BR(2)	Y Coordinate
BR(3)	Z Coordinate
XS(20)	Intial set of x values (radii of desired starting point of a field line)
YS(20)	Intial set of y values (height off midplane)
RADIUS	Major radius of the device in meters
ASPECT	The aspect ratio of the plasma
SCALE	The graph scaling. Equals 1.0 for 1.0" on graph to equal 1.0 meter on device.
NLINE	Number of field lines to be traced. Maximum is 20.
NCOIL	The number of current segments in the divertor. Maximum is 20.
CURRENT	The current in the divertor. All V7'S are multiplied by this number.
TOL	Integrator tolerance
BPA	A variable to be used in MAGFLD. Currently unused.
BZA	A variable to be used in the subr MAGFLD. Currently it is the toroidal field in tesla.

V(7,20) The array that contains the current segment information.

V(1,N) The X coordinate of the starting point of current segment N.

V(2,N) The Y coordinate of the starting point of current segment N.

V(3,N) The Z coordinate of the starting point of current segment N.

V(4,N) The X coordinate of the ending point of current segment N.

V(5,N) The Y coordinate of the ending point of current segment N.

V(6,N) The Z coordinate of the ending point of current segment N.

V(7,N) The Relative current in coil segment N thats flows from start to end.

G(100,2) Contains the auxiliary graphing coordinates.

G(N,1) X coordinate.

G(N,2) Z corrdinate.

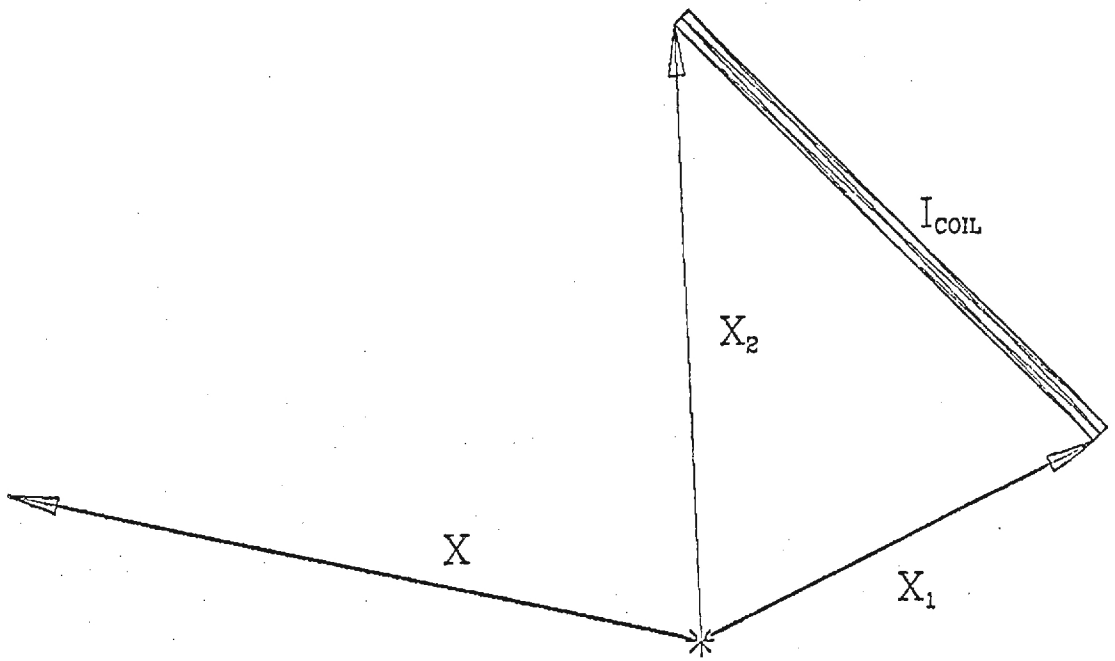

Figure 1

```
/JOB
/NOSEQ
FOLLOW,T1000.
USER.
G,DIVERT,FNMLIB/UN=NE10109.
AT,CALCOMP,IMSLIB/UN=LIBRARY.
NOEXIT.
FTN,I=DIVERT,L=0,ER,REW,T,PMD.
LOSET(LIB=CALCOMP/IMSLIB/FNMLIB).
LGO,OP=F.
R,CLT.
C,CLT,OUTPUT.
PLOTCV,TAPE3.
/EOR
 $PRAM
 RADIUS=5.0,
 ASPECT=3.8,
 SCALE=0.62,
 CURRENT=5.0,
 $
 $IN
 TOL=1.E-4,
 NCOIL=7,
 V(1,1)=7.1, -.4, 0., 7.1, .4, 0., 2.,
 V(1,2)=7.1,  .4, 0., 6.4, .4, -.8, 1.,
 V(1,3)=6.4,  .4, -.8, 6.4, -.4, -.8, 1.,
 V(1,4)=6.4, -.4, -.8, 7.1, -.4,  .0, 1.,
 V(1,5)=7.1,  .4,  .0, 6.4,  .4,  .8, 1.,
 V(1,6)=6.4,  .4,  .8, 6.4, -.4,  .8, 1.,
 V(1,7)=6.4, -.4,  .8, 7.1, -.4,  .0, 1.,
 NLINE=11,
 $
 $GRAPH
 G(1,1)=4.89, 5.86, 6.59, 7.28, 7.28, 6.59, 6.22, 6.94, 7.84,
 9.0, 5.59, 5.37, 6.22, 5.82, 1.E3, 5.46, 6.54,
 7.03, 8.02, 8.02, 7.03, 1.E4,
 G(1,2)=4.48, 3.31, 1.6, 1.6, -1.6, -1.6, -1.88, -3.14, -2.60,
 -4.57, -4.66, -3.99, -3.58, -2.87, 1.E3, 4.93, 3.54,
 2.20, 2.20, -2.20, -2.20, 1.E4,
 $
APRIL 1980 TEST
YES
ANGLE BUNDLE DIVERTOR - TWO LOOPS WITH RECTANGULAR CROSS SECTION
TEST CASE
PLASMA WITH TOROIDAL FIELD ONLY
```

NOTES
ANGLE BUNDLE DIVERTOR – TWO LOOPS WITH RECTANGULAR CROSS SECTION
TEST CASE
PLASMA WITH TOROIDAL FIELD ONLY
RADIUS = 5.000E+00, ASPECT = 3.800E+00
CURRENT = 5.000E+00, BZA = 5.000E+00, COIL SEGMENTS = 7

APRIL 1980 TEST

METER

BUNDLE DIVERTER FIELD LINES

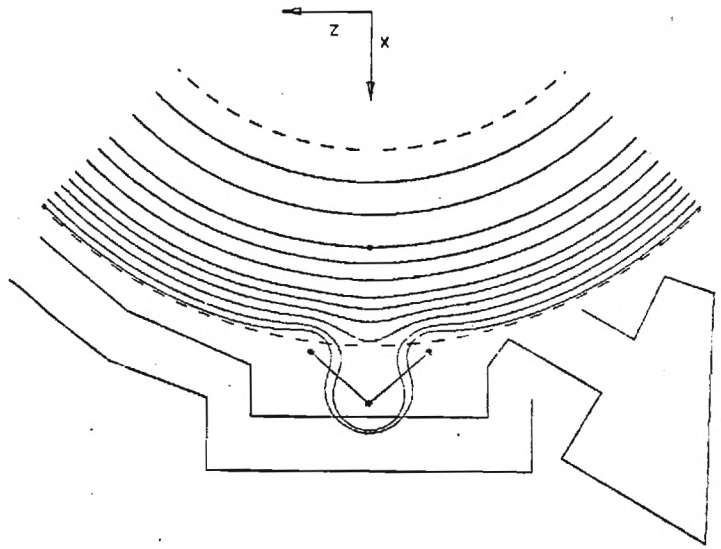

SIDE VIEW
OF COILS

RIPPLE ON AXIS POS 7.762E-01% NEG -1.095E-01%

Figure 2

```
/JOB
/NOSEQ
FOLLOW,T1000.
USER.
G,DIVERT,RNMLIB/UN=NE101G8.
AT,CALCOMP,IMSLIB/UN=LIBRARY.
NOEXIT.
FTN,I=DIVERT,L=0,ER,REW,T,PMD.
LDSET(LIB=CALCOMP/IMSLIB/RNMLIB).
LGO,OP=F.
R,OJT.
C,OUT,OUTPUT.
PLOTCV,TAPE3.
/EOR
 $PRAM
 RADIUS=5.0,
 ASPECT=3.8,
 SCALE=0.62,
 CURRENT=5.0,
 $
 $IN
 TOL=1.E-4,
 NCOIL=7,
 V(1,1)=6.8, -.4, 0., 6.8, .4, 0., 2.,
 V(1,2)=6.8,  .4, 0., 6.8, .4, -.8, 1.,
 V(1,3)=6.8,  .4, -.8, 6.8, -.4, -.8, 1.,
 V(1,4)=6.8, -.4, -.8, 6.8, -.4,  .0, 1.,
 V(1,5)=6.8,  .4,  .0, 6.8,  .4,  .8, 1.,
 V(1,6)=6.8,  .4,  .8, 6.8, -.4,  .8, 1.,
 V(1,7)=6.8, -.4,  .8, 6.8, -.4,  .0, 1.,
 NLINE=11,
 $
 $GRAPH
 G(1,1)=4.89, 5.86, 6.59, 7.28, 7.28, 6.59, 6.22, 6.94, 7.84,
 9.0, 5.59, 5.37, 6.22, 5.82, 1.E3, 5.46, 5.54,
 7.03, 8.02, 8.02, 7.03, 1.E4,
 G(1,2)=4.48, 3.31, 1.6, 1.6, -1.6, -1.6, -1.88, -3.14, -2.60,
 -4.57, -4.66, -3.99, -3.58, -2.87, 1.E3, 4.93, 3.54,
 2.20, 2.20, -2.20, -2.20, 1.E4,
 $
APRIL 1980 TEST
YES
PLANAR BUNDLE DIVERTOR - TWO LOOPS WITH RECTANGULAR CROSS SECTION
TEST CASE
PLASMA WITH TOROIDAL FIELD ONLY
```

NOTES

PLANAR BUNDLE DIVERTOR - TWO LOOPS WITH RECTANGULAR CROSS SECTION APRIL 1980 TEST

TEST CASE

PLASMA WITH TOROIDAL FIELD ONLY

RADIUS = 5.000E+00, ASPECT = 3.800E+00

CURRENT = 5.000E+00, BOA = 5.000E+00, COIL SEGMENTS = 7

METER

BUNDLE DIVERTER FIELD LINES

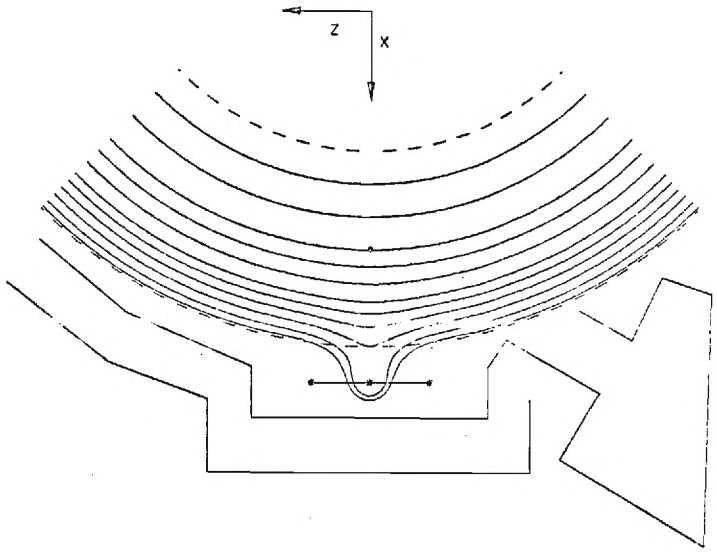

SIDE VIEW OF COILS

RIPPLE ON AXIS POS 2.930E-01% NEG -1.300E+00%

Figure 3

```
/JOB
/NOSEQ
FOLLOW,T1000.
USER.
G,DIVERT,RAMLIB/UN=AE1016R.
AT,CALCOMP,IMSLIB/LN=LIBRARY.
NOEXIT.
FTN,I=DIVERT,L=0,ER,REW,T,FMD.
LDSET(LIB=CALCOMP/IMSLIB/RAMLIB).
LGO,OP=F.
R,CLT.
C,CLT,OLTPLT.
PLOTCV,TAPE3.
/EOP
 $FRAM
 RADIUS=5.0,
 ASPECT=3.8,
 SCALE=0.62,
 CURRENT=5.0,
 $
 $IN
 TOL=1.E-4,
 NCOIL=7,
 V(1,1)=6.4, -.4, 0., 6.4, .4, 0., 2.,
 V(1,2)=6.4,  .4, 0., 7.1, .4, -.8, 1.,
 V(1,3)=7.1,  .4, -.8, 7.1, -.4, -.8, 1.,
 V(1,4)=7.1, -.4, -.8, 6.4, -.4,  .0, 1.,
 V(1,5)=6.4,  .4,  .0, 7.1,  .4,  .8, 1.,
 V(1,6)=7.1,  .4,  .8, 7.1, -.4,  .8, 1.,
 V(1,7)=7.1, -.4,  .8, 6.4, -.4,  .0, 1.,
 NLINE=11,
 $
 $GRAPH
 G(1,1)=4.89, 5.86, 6.59, 7.28, 7.28, 6.59, 6.22, 6.94, 7.84,
 9.0, 5.59, 5.37, 6.22, 5.82, 1.E3, 5.46, 6.54,
 7.03, 8.02, 8.02, 7.03, 1.E4,
 G(1,2)=4.48, 3.31, 1.6, 1.6, -1.6, -1.6, -1.88, -3.14, -2.60,
 -4.57, -4.66, -3.99, -3.58, -2.87, 1.E3, 4.93, 3.54,
 2.20, 2.20, -2.20, -2.20, 1.E4,
 $
APRIL 1980 TEST
YES
ANGLE BUNDLE DIVERTOR - TWO LOOPS WITH RECTANGULAR CROSS SECTION
TEST CASE
PLASMA WITH TOROIDAL FIELD ONLY
```

NOTES
ANGLE BUNDLE DIVERTOR – TWO LOOPS WITH RECTANGULAR CROSS SECTION
TEST CASE
PLASMA WITH TOROIDAL FIELD ONLY
RADIUS = 5.000E+00, ASPECT = 3.800E+00
CURRENT = 5.000E+00, BZA = 5.000E+00, COIL SEGMENTS = 7

APRIL 1980 TEST

METER

BUNDLE DIVERTER FIELD LINES

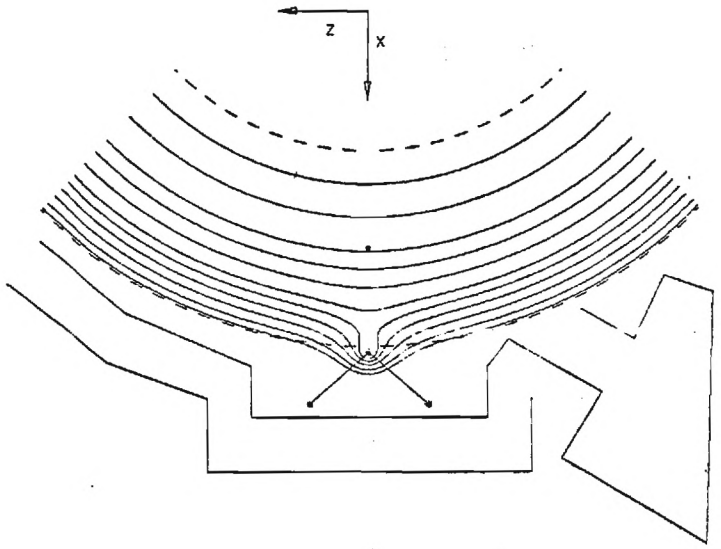

SIDE VIEW
OF COILS

RIPPLE ON AXIS POS 5.375E-01% NEG -3.957E+00%

Figure 4

APPENDIX

Computer Program DIVERT

```
1      PROGRAM DIVERT (INPUT,OUTPUT,OUT
     & ,TAPE5=INPUT,TAPE6=OUT,TAPE7=OUT,TAPE8=INPUT)
C
C    *** PROGRAM DIVERT BY R. N. MORRIS AND G. BATEMAN.  APRIL 1980 ***
C    *** GEORGIA TECH, ATLANTA GEORGIA ***
C
C*****************************************************************
C*                                                               *
C*  THIS PROGRAM TRACES MAGNETIC FIELD LINES THROUGH             *
C*  A DIVERTOR.  THE MAGNETIC FIELD EQUATIONS ARE                *
C*  IN SUBR MAGFLD.  SUBMIT USING FILE CSUB                      *
C*                                                               *
C*****************************************************************
C   BF(1) IS X
C   BF(2) IS Y
C   BF(3) IS Z
C   SUBR MAGFLD CONTAINS THE EQUATIONS FOR THE MAGNETIC
C      FIELD.  THIS SUBR IS TO BE MODIFIED BY THE USER FOR THE
C     SPECIFIC PROBLEM ENCOUNTERED.  IT CURRENTLY IS SET UP TO
C     HANDLE A MAGNETIC CONFIGURATION MADE OF UP TO 20 STRAIGHT
C     LINE SEGMENTS.
C*****************************************************************
C
C                     INPUTS
C
C   XS(20) IS THE INITIAL SET OF X VALUES (RADII OF DESIRED
C        STARTING POINT OF FIELD LINE)
C   YS(20) IS THE INITIAL SET OF Y VALUES (HEIGHT OFF MIDPLANE)
C        BOTH ARRAYS HAVE DEFAULT VALUES WITHIN THE PROGRAM
C        -- 11 FIELD LINES WITH DECREASING SPACING WITH INCREASING
C           RADII
C        --MAGNETIC AXIS     XS(-) = RADIUS, YS(-) = 0.0
C   RADIUS IS THE MAJOR RADIUS OF THE DEVICE  (IN METERS)
C   ASPECT IS THE ASPECT RATIO OF THE PLASMA
C   SCALE IS THE GRAPH SCALING. = 1 FOR 1" ON PLOT TO EQUAL
C        1 METER IN DEVICE.
C   NLINE IS THE NUMBER OF FIELD LINES TO BE TRACED.  MUST
C        BE LESS THAN 21
C   NCOIL IS THE NUMBER OF CURRENT SEGMENTS IN THE DIVERTOR
C        COIL.  MUST BE LESS THAN 21.
C   V(1,N),V(2,N),V(3,N)   V(4,N),V(5,N),V(6,N)   VERTEX
C        COORDINATES FOR THE END POINTS OF EACH STRAIGHT COIL
C        LEG IN THE BUNDLE DIVERTOR.
C        -STARTING POINT OF LINE SEGMENT N. (CURRENT FLOWS TOWARD
C         THE END POINT)
C         V(1,N) IS X
C         V(2,N) IS Y
C         V(3,N) IS Z
C        -ENDING POINT OF LINE SEGMENT N.
C         V(4,N) IS X
C         V(5,N) IS Y
C         V(6,N) IS Z
C   V(7,N) IS THE RELATIVE CURRENT IN COIL SEGMENT N.
C   CURRENT IS THE NOMINAL CURRENT IN THE DIVERTOR.  ALL V7'S ARE
C        MULTIPLIED BY THIS NUMBER.  CURRENT IS IN MEGAMPS.
C   TOL IS THE INTEGATOR TOLERANCE.
C   BZA AND BPA ARE FREE VARIABLES TO BE USED IN SUBR MAGFLD
C        FOR THE TOKAMAK MAGNETIC FIELDS.
C
C   ALL THE ABOVE VALUES HAVE DEFAULT VALUES..
C
C
C*****************************************************************
C
```

```
C                  NAMELISTS
C
C       IN
C*********************
C
C   NLINE, XS(20), YS(20), NCOIL, V(7,20), TOL, BPA, BZA
C
C
C     PRAM
C*********************
C
C   RADIUS, ASPECT, SCALE, CURRENT
C
C
C     GRAPH
C*********************
C
C  G
C
C*****************************************************************
C
C         NOTES AND GRAPHICS
C
C    TO USE THE GRAPHING.  G(-,1) IS THE X VALUE, G(-,2) IS THE
C   Z VALUE.   THE G ARRAY CAN HAVE A MAXIMUM OF 100 VALUES G(100,2)
C   THE TWO IMPORTANT CONTROL VALUES ARE 1.E3 AND 1.E4.  IF G(-,1)
C   IS EQUAL TO 1.E4 THE GRAPHING IS TERMINATED.  IF G(N,1) IS EQUAL
C   TO 1.E3 THE PEN IS LIFTED FOR THE MOVE FROM G(N-1,1) TO
C   G(N+1,1).  OTHERWISE A LINE IS DRAWN FROM G(N,1) , G(N,2)  TO
C   G(N+1,1) , G(N+1,2).
C
C     TO USE THE NOTE CAPABILITY.  AFTER ALL THE NAMELISTS
C   HAVE BEEN ENTERED, THE NEXT ITEM TO BE READ IS THE RUN NUMBER
C   THIS ALPHANUMERIC INPUT CAN BE UP TO 20 CHARACTERS LONG AND
C   MUST BE ENTERED (IT CAN BE ALL BLANKS).  AFTER THIS THE FOLLOWING
C   LINE SHOULD CONTAIN EITHER A YES OR NO.  IF A NO IS ENTERED, THE
C   DATA INPUT IS COMPLETE.  IF A YES IS ENTERED, THE NEXT THREE
C   LINES CONTAIN ANY ALPHANUMERIC DATA (UP TO 65 CHARACTERS EACH).  PAD
C   WITH BLANK LINES IF NECESSARY TO COMPLETE ALL THREE LINES.
C   IF YOU ARE HAVING THE COMPUTER PROMPT THE TERMINAL, JUST
C   FOLLOW THOSE INSTRUCTIONS.
C
C*****************************************************************
      DIMENSION BF(3), SCRATCH(8)
      COMMON /PAR/ PI
      COMMON /FIELD/ NLINE, XS(20), YS(20)
     & ,BAMAX,XBAMAX,YBAMAX,ZBAMAX ,BAMIN,XBAMIN,YBAMIN,ZBAMIN
     & ,NCOIL, V(7,20), CURRENT
     & ,TOL,RADIUS,ASPECT,SCALE,XREF,YREF,BPA,BZA
C
      COMMON /INT/ XVALUE
C
      DATA PI/3.14159265359/ , IW/6/
C
C   SET UP DATA
C
      CALL DATAIN
C
C   SETUP GRAPH AND INITIALIZE VALUES
C
      CALL STARTP(2)
C
      CALL SETUP
C
C   DETERMINE FIELD LINE STEPS
C
```

```
      DS = .032 / SCALE
C
C   SELECT STARTING POINTS AND INITIALIZE VALUES
C
      DO 50 M=1,NLINE
C
        BAMAX  = 0.
        BAMIN  = 100.
        ISWITCH = 0
        BF(1)  = .707 * XS(M)
        BF(2)  = YS(M)
        BF(3)  = BF(1)
        ZEND   = - BF(1)
        XP     = (BF(1) - RADIUS) * SCALE
        YP     = - BF(3) * SCALE
        CALL PLOT(XP,YP,3)
C
C   INTEGRATE AROUND THROUGH THE DIVERTER AND DRAW FIELD LINES
C
        BEGIN = 0.0
        DO 10 I=1,10000
          FINISH = DS + BEGIN
          CALL DSOLVE(BEGIN,FINISH,BF,TOL,ISWITCH,IW)
          XP = (BF(1) - RADIUS) * SCALE
          YP = - BF(3) * SCALE
          CALL PLOT(XP,YP,2)
          IF((BF(3).LT.0.0).AND.(ABS(BF(3)).GT.ABS(BF(1)))) GO TO 20
          BEGIN = FINISH
 10     ISWITCH = 1
C
C   WRITE OUT MAX AND MIN B FIELD ON THE GIVEN LINE
C
 20     WRITE (6,30) M,XS(M),YS(M),BAMAX,BAMIN
 30     FORMAT (1X,I3,1P7E13.5)
C
C   COMPUTE RIPPLE ON AXIS AND WRITE OUT ON GRAPH.
C
        IF (M .NE. 1) GO TO 50
        RPLPOS = 100. * (BAMAX-BZA) / BZA
        RPLNEG = 100. * (BAMIN-BZA) / BZA
        XPLOT1 = 10.0 - XREF
        YPLOT1 = 1. - YREF
        ENCODE(20,40,SRATCH) RPLPOS, RPLNEG
 40     FORMAT("!RIPPLE ON AXIS",5X,"POS",1X,1PE11.3
     &    ,"<#J",5X,"!>NEG",1X,1PE11.3,"<#J")
        CALL SYMBOL(XPLOT1,YPLOT1,.080,SRATCH,90.0,63)
C
 50   CONTINUE
C
      CALL ENDP
C
      STOP
      END
C-----------------------------------------------------------------
      SUBROUTINE DATAIN
C
C   THIS SUBR HANDLES THE DATA
C
      COMMON /PAR/ PI
C
      COMMON /TEXT/ NOTE1(7) , NOTE2(7) , NOTE3(7) , NRUN(2), G(100,2)
C
      COMMON /FIELD/ NLINE, XS(20), YS(20)
     & ,BAMAX,XBAMAX,YBAMAX,ZBAMAX ,BAMIN,XBAMIN,YBAMIN,ZBAMIN
     & ,NCOIL, V(7,20), CURRENT
     & ,TOL,RADIUS,ASPECT,SCALE,XREF,YREF,BPA,BZA
C
      NAMELIST /IN/ NLINE, XS, YS, NCOIL, V, TOL, BPA, BZA
C
      NAMELIST /PRAM/ RADIUS, ASPECT, SCALE, CURRENT
C
      NAMELIST /GRAPH/ G
C
C   DEFAULTS
C
        TOL     = 1.E-7
        RADIUS  = 3.
        ASPECT  = 3.0
        BPA     = 1.0
        BZA     = 5.
        SCALE   = 1.0
        NLINE   = 1
        NCOIL   = 1
        CURRENT = 5.0
        G(1,1)  = 1.E4
C
        DO 10 I=1,11
 10     YS(I) = 0.0
C
        V(1,1) = 4.
        V(2,1) = -1.
        V(3,1) = 0.
        V(4,1) = 4.
        V(5,1) = 1.
        V(6,1) = 0.
        V(7,1) = 1.
C
        DO 30 I=1,7
            NOTE1(I) = "           "
            NOTE2(I) = "           "
            NOTE3(I) = "           "
 30     CONTINUE
C
C   READ IN DATA AND COMPUTE FIELD LINE SPACING
C
        READ (5,PRAM)
C
        XS(1)   = RADIUS
C
        SPACE   = RADIUS/(ASPECT*3.0)
        XS(2)   = RADIUS - 2.0*SPACE
        XS(3)   = XS(2) + SPACE
C
        SPACE   = RADIUS/(ASPECT*6.0)
        XS(4)   = RADIUS + SPACE
        XS(5)   = XS(4) + SPACE
        XS(6)   = XS(5) + SPACE
C
        SPACE   = RADIUS/(ASPECT*10.0)
        XS(7)   = XS(6) + SPACE
        XS(8)   = XS(7) + SPACE
        XS(9)   = XS(8) + SPACE
        XS(10)  = XS(9) + SPACE
        XS(11)  = XS(10) + SPACE*0.75
C
        READ(5,IN)
        READ(5,GRAPH)
C
```

```
C   READ RUN NUMBER
C
      WRITE(7,40)
 40    FORMAT(2X,"TYPE IN RUN NUMBER")
      READ(8,50) (NRUN(I),I=1,2)
 50   FORMAT(2A10)
C
C   READ NOTES
C
      WRITE(7,60)
 60   FORMAT(2X,"IF YOU WISH TO ADD NOTES, TYPE IN YES",/,
     & 2X,"OTHERWISE TYPE IN NO")
C
      READ(8,70) ANS
 70   FORMAT(A1)
C
      IF(ANS.NE."Y") GO TO 100
C
      WRITE(7,80)
 80   FORMAT(2X,"TYPE IN NOTES, 3 LINES MAX, 65 CHARACTERS",
     & /,2X,"PER LINE MAX.  IF YOU INPUT LESS THAN 3 LINES",
     & /,2X,"TYPE A LINE OF BLANKS FOR THE REMAINING LINE(S)")
C
      READ(8,90) (NOTE1(I),I=1,7)
 90   FORMAT(7A10)
      READ(8,90) (NOTE2(I),I=1,7)
      READ(8,90) (NOTE3(I),I=1,7)
C
C   WRITE OUT HEADER
C
 100   CALL STAR(1,6)
      WRITE(6,110)
 110   FORMAT(/,10X,"MORRIS AND BATEMAN FIELD LINE TRACING CODE",
     & /,15X,"GEORGIA TECH 1979",/)
      CALL STAR(1,6)
      CALL SKIP(2,6)
C
C   WRITE OUT NOTES
C
      WRITE(6,120)
 120   FORMAT(2X,"NOTES:",/)
C
      WRITE(6,130) (NOTE1(I),I=1,7)
      WRITE(6,130) (NOTE2(I),I=1,7)
      WRITE(6,130) (NOTE3(I),I=1,7)
 130   FORMAT(2X,7A10)
      CALL SKIP(2,6)
C
C   WRITE OUT NAMELISTS
C
      WRITE(6,PRAM)
      WRITE(6,IN)
      WRITE(6,GRAPH)
      CALL SKIP(2,6)
C
C   WRITE OUT OTHER HEADER INFORMATION
C
      WRITE(6,140)
 140  FORMAT(/,3X,"M",6X,"XS(M)",6X,"YS(M)",8X
     &      ,"BAMAX",6X,"BAMIN")
      RETURN
      END
C-----------------------------------------------------------------------
      SUBROUTINE OSCLVE(XSTART,XEND,BF,TOL,ISWITCH,IW)
C
C   THIS SUBR USES THE IMSL SUBR DREBS TO INTEGRATE
C    BETWEEN XSTART AND XEND
C
C   XSTART IS THE BEGINNING VALUE OF THE INTEGRATION
C   XEND IS THE FINAL VALUE OF THE INTEGRATION LIMIT
C   BF IS THE VALUE OF THE FUNCTION AT XEND
C   TOL IS THE INTEGRATING TOLERANCE
C   ISWITCH    =  0 FOR FIRST CALL
C              =  1 FOR REMAINING CALLS
C   IW IS THE LOGICAL UNIT ERRORS ARE WRITTEN ON
C
      EXTERNAL OFIELD
      DIMENSION BF(3) , R(3) , S(3) , WK(87)
      COMMON /INT/ XVALUE
C
      IF(ISWITCH.NE.0) GO TO 10
C
C   INITIALIZE VALUES
C
      JM        = 6
      INC       = 2
      JSTART    = 0
      N         = 3
      S(1)      = BF(1)
      S(2)      = BF(2)
      S(3)      = BF(3)
      SAVE      = XEND - XSTART
      HMIN      = 1.E-9
      ERROR     = 0.5 * HMIN
      XVALUE    = XSTART
C
  10  CONTINUE
C
      H = XEND - XVALUE
      IF(ABS(SAVE).LT.ABS(H)) H = SAVE
C
C   INTEGRATE TO THE END POINT
C
      DO 30 I=1,1000
          CALL DREBS(OFIELD,BF,XVALUE,N,JM,INC,JSTART,H,HMIN,TOL,
     &      R,S,WK,IER)
          IF(IER.NE.0) GO TO 40
          TEMP = XEND - XVALUE
          IF(ABS(TEMP).LT.ERROR) RETURN

          SAVE = H
          IF(ABS(TEMP).GT.ABS(H)) GO TO 30
          H = TEMP
 30   CONTINUE
C
C   ERROR EXIT
C
 40   CALL SYMBOL(-2.0,-0.40,0.20,"*ABORT",0.0,6)
      CALL ENDP
      CALL STAR(2,IW)
      WRITE(IW,50) XVALUE , H
 50   FORMAT(//,2X,"PROBLEM AT Z = ",1PE11.3,2X,
     & "STEP SIZE = ",1PE11.3,//,5X,
     & "********SYSTEM ABORT********",///)
C
      CALL STAR(2,IW)
C
      STOP
```

```
      END
C-----------------------------------------------------------------------
      SUBROUTIN  SETUP
      DIMENSION TITLE(12)
C
      COMMON /TEXT/ NOTE1(7) , NOTE2(7) , NOTE3(7) , NRUN(2), G(100,2)
C
      COMMON /FIELD/ NLINE, XS(20), YS(20)
     & ,BAMAX,XBAMAX,YBAMAX,ZBAMAX ,BAMIN,XBAMIN,YBAMIN,ZBAMIN
     & ,NCOIL, V(7,20), CURRENT
     & ,TCL,RADIUS,ASPECT,SCALE,XREF,YREF,BPA,BZA
C
C   THIS SUBR PREPARES THE GRAPH FORMAT
C    IT DRAWS THE MARGINS AND LABELS THE GRAPHS
C
C   DRAW MARGIN
C
      CALL MARGIN
C
C   LOCATE AND DRAW LABEL
C
      CALL SYMBOL(2.30,1.85,.160,
     &  "!BUNDLE DIVERTER FIELD LINES",90.0,28)
C
C   WRITE OUT NOTES AND OTHER PARAMETERS ON GRAPH
C
C   SCALE LINE
C
      CALL SYMBOL(1.50,6.00,.100,13,90.0,-1)
      XC1 = 6.00 + SCALE
      CALL SYMBOL(1.50,XC1,.100,13,90.0,-1)
      CALL PLOT(1.50,6.00,3)
      CALL PLOT(1.50,XC1,2)
      XC1 = 6.00 + SCALE/2.0 - .2
      CALL SYMBOL(1.72,XC1,.080,"!METER",90.0,6)
C
C   NOTES
C
      CALL SYMBOL(0.75,1.00,.080,"NOTES",90.0,6)
      CALL PLOT(0.78,1.00,3)
      CALL PLOT(0.78,1.48,2)
      CALL SYMBOL(0.92,1.00,.080,NOTE1,90.0,65)
      CALL SYMBOL(1.06,1.00,.080,NOTE2,90.0,65)
      CALL SYMBOL(1.20,1.00,.080,NOTE3,90.0,65)
      ENCODE(120,5,TITLE)RADIUS, ASPECT
    5 FORMAT("RADIUS =",1X,1PE10.3,",",1X,"ASPECT =",1X,1PE10.3)
      CALL SYMBOL(1.34,1.00,.080,TITLE,90.0,65)
      ENCODE(120,10,TITLE)CURRENT, BZA, NCOIL
   10 FORMAT("CURRENT =",1X,1PE10.3,",",1X,"BZA =",1X,1PE10.3
     &       ,",",1X,"COIL SEGMENTS =",1X,I2)
      CALL SYMBOL(1.48,1.00,.080,TITLE,90.0,65)
      CALL SYMBOL(8.44,1.00,0.080,"SIDE VIEW",90.0,9)
      CALL SYMBOL(8.56,1.00,0.080,"OF COILS" ,90.0,8)
C
C   RUN NUMBER
C
      CALL RECT(0.75,5.98,1.60,0.16,0.0,3)
      ENCODE (120,20,TITLE) NRUN(1),NRUN(2)
   20 FORMAT (2A10)
      CALL SYMBOL(0.87,6.02,.080,TITLE,90.0,18)
C
C   DRAW OUT AXIS
C
      CALL ARCHD(2.75,4.25,3.50,4.25,0.15,0.05,12)
      CALL ARCHD(2.75,4.25,2.75,3.50,0.15,0.05,12)
      CALL SYMBOL(3.05,4.32,0.080,"X",90.0,1)
      CALL SYMBOL(2.95,3.90,0.080,"Z",90.0,1)
C
C   DRAW OUT TOROID AND COIL CONFIGURATION
C
C   DRAW TOROID
C
      A    = RADIUS/ASPECT
      RIN  = RADIUS - A
      ROUT = RADIUS + A
      XREF = 3.25 + (RIN*0.293 + .8) * SCALE
      YREF = 4.25
      CALL PLOT(XREF,YREF,-3)
      CALL SYMBOL(0.0,0.0,0.045,14,90.0,-1)
      XC1  = -A * SCALE
      RAD  = RIN * SCALE
      CALL CIRCLE(XC1,0.0,0.0,45.0,RAD,RAD,0.5)
      CALL CIRCLE(XC1,0.0,0.0,-45.0,RAD,RAD,0.5)
      XC1  = -XC1
      RAD  = ROUT * SCALE
      CALL CIRCLE(XC1,0.0,0.0,45.0,RAD,RAD,0.5)
      CALL CIRCLE(XC1,0.0,0.0,-45.0,RAD,RAD,0.5)
C
C   DRAW COILS (TOP VIEW)
C
      DO 40 I=1,NCOIL
        XC1 = (V(1,I)-RADIUS)*SCALE
        YC1 = -V(3,I)*SCALE
        XC2 = (V(4,I)-RADIUS)*SCALE
        YC2 = -V(6,I)*SCALE
        IF((XC1.EQ.XC2).AND.(YC1.EQ.YC2)) GO TO 30
        CALL PLOT(XC1,YC1,3)
        CALL PLOT(XC2,YC2,2)
        CALL SYMBOL(XC1,YC1,0.060,11,0.0,-1)
   30   CALL SYMBOL(XC2,YC2,0.060,11,0.0,-1)
   40 CONTINUE
C
C   DRAW COILS (SIDE VIEW)
C
      DO 50 I=1,NCOIL
        XC1 = -V(2,I) * SCALE - XREF + 8.50
        YC1 = -V(3,I) * SCALE
        XC2 = -V(5,I) * SCALE - XREF + 8.50
        YC2 = -V(6,I) * SCALE
        IF((XC1.EQ.XC2).AND.(YC1.EQ.YC2)) GO TO 45
        CALL PLOT(XC1,YC1,3)
        CALL PLOT(XC2,YC2,2)
   45   CALL SYMBOL(XC1,YC1,0.060,11,0.0,-1)
        CALL SYMBOL(XC2,YC2,0.060,11,0.0,-1)
   50 CONTINUE
C
C   DRAW OUT THE HARDWARE AROUND THE DIVERTOR
C
      J = 3
      DO 60 I=1,100
        IF(G(I,1).GT.9000.0) GO TO 70
        IF(G(I,1).GT.900.0)  J = 3
        IF(G(I,1).GT.900.0) GO TO 60
        XC1 = (G(I,1) - RADIUS)*SCALE
        YC1 = -G(I,2)*SCALE
        CALL PLOT(XC1,YC1,J)
        J = 2
   60 CONTINUE
   70 RETURN
      END
```

```
C-------------------------------------------------------
      SUBROUTIN  DFIELD (N,S,F,FP)
      DIMENSION F(N), FP(N)
C
C   THIS IS THE DIFF EQ SET FOR THE FIELD LINES
C  IN A TOROID GIVEN ANY THREE COORDINATES (X,Y,Z)
C  F(1) = X , F(2) = Y , F(3) = Z
C
      COMMON /FIELD/ NLINE, XS(20), YS(20)
     & ,BAMAX,XBAMAX,YBAMAX,ZBAMAX ,BAMIN,XBAMIN,YBAMIN,ZBAMIN
     & ,NCOIL, V(7,20), CURRENT
     & ,TCL,RADIUS,ASPECT,SCALE,XREF,YREF,BPA,BZA
C
      COMMON /PAR/ PI
C
C DETERMINE FIELD COMPONENTS
C
      CALL MAGFLD(F(1),F(2),F(3),BX,BY,BZ,B)
C
C  DIFF EQUATION FOR FIELD LINE IN CYLINDER
C
      FP(1) = BX / B
      FP(2) = BY / B
      FP(3) = BZ / B
C
      RETURN
      END
C-------------------------------------------------------------------
      SUBROUTINE MAGFLD(X,Y,Z,BX,BY,BZ,B)
C
C  THIS SUBR COMPUTE THE MAGNETIC FIELD COMPONENTS OF A TOROIDIAL
C   FIELD WITH COMPONENTS IN THE X,Y AND Z DIRECTION
C
      COMMON /FIELD/ NLINE, XS(20), YS(20)
     & ,BAMAX,XBAMAX,YBAMAX,ZBAMAX ,BAMIN,XBAMIN,YBAMIN,ZBAMIN
     & ,NCOIL, V(7,20), CURRENT
     & ,TCL,RADIUS,ASPECT,SCALE,XREF,YREF,BPA,BZA
C
C   COMPUTE TOROID FIELD
C
      DEM = (Z*Z + X*X)
      BX = BZA * Z * RADIUS / DEM
      BY = 0.0
      BZ = - BZA * X * RADIUS / DEM
C
C   COMPUTE FIELD FROM DIVERTOR
C
      DO 20 N=1,NCOIL
        V1X = V(1,N) - X
        V1Y = V(2,N) - Y
        V1Z = V(3,N) - Z
        V1A = SQRT (V1X*V1X + V1Y*V1Y + V1Z*V1Z)
C
        V2X = V(4,N) - X
        V2Y = V(5,N) - Y
        V2Z = V(6,N) - Z
        V2A = SQRT (V2X*V2X + V2Y*V2Y + V2Z*V2Z)
C
        V3X = V(4,N) - V(1,N)
        V3Y = V(5,N) - V(2,N)
        V3Z = V(6,N) - V(3,N)
C
        CX = V3Y*V1Z - V3Z*V1Y
        CY = V3Z*V1X - V3X*V1Z
        CZ = V3X*V1Y - V3Y*V1X
        CASC = CX*CX + CY*CY + CZ*CZ
C
        F = CURRENT * V(7,N) * (((V3X*V1X+V3Y*V1Y+V3Z*V1Z
     &    - ((V2X*V2X+V2Y*V2Y+V2Z*V2Z)/V2A)) / (CASC * 10
C
        BX = BX + CX*F
        BY = BY + CY*F
        BZ = BZ + CZ*F
 20   CONTINUE
C
C   KEEP TRACK OF FIELD RIPPLE.  DETERMINE FIELD
C   STRENGTH AND IF IT IS AN EXTREME, SAVE THE FIELD
C   POSITIONS.
C
      B = SQRT (BX*BX + BY*BY + BZ*BZ)
C
      IF (B .LT. BAMAX) GO TO 40
      BAMAX = B
      XBAMAX = X
      YBAMAX = Y
      ZBAMAX = Z
C
 40   CONTINUE
      IF (B .GT. BAMIN) RETURN
      BAMIN = B
      XBAMIN = X
      YBAMIN = Y
      ZBAMIN = Z
C
      RETURN
      END
```

```
C***     THESE SUBR ARE FROM RAMLIB *****
C
C*************************************************************
C***
C***   LIBRARY
C***
C*************************************************************
C***
C***   GRAPHING
C***
C***   TO GRAPH, FIRST CALL STARTP WITH THE TOTAL NUMBER
C***   OF GRAPHS YOU PLAN TO MAKE.  THEN CALL PLOTEP OR
C***   PLOTON.  AFTER THE PLOTTING IS DONE CALL ENDP.
C***   FINALLY SEND TAPE3 TO THE PLOTTING DEVICE.
C***
C*************************************************************
      SUBROUTINE STARTP(N)
      DIMENSION IBUFF(512)
C
C    THIS FUNCTION OPENS UP THE PLOT FILE ON UNIT 3
C      AND SETS THE PAPER LENGTH
C
C       N IS THE TOTAL NUMBER OF GRAPHS TO BE MADE
C
      CALL PLOTS(IBUFF,512,3,0)
      R = N * 15.
      CALL PLOTMX(R)
      END
C-------------------------------------------------------------
      SUBROUTINE ENDP
C
C    THIS FUNCTION CLOSES THE PLOT FILE
C
      CALL PLOT(0.,0.,999)
      RETURN
      END
C*************************************************************
C****
C****   FUNCTION ROUTINES
C****
C*************************************************************
      SUBROUTINE SKIP(I,NOUT)
C
C    THIS SUBR SKIPS I LINES ON UNIT NOUT
C
      DO 10 J=1,I
 10   WRITE(NOUT,20)
 20   FORMAT(/)
      RETURN
      END
C-------------------------------------------------------------
      SUBROUTINE STAR(I,NOUT)
C
C    THIS SUBR PRINTS I LINES OF STARS ON UNIT NOUT
C
      DO 10 J=1,I
 10   WRITE(NOUT,20)
 20   FORMAT("**************************************************"
     $ ,"**************************************************")
      RETURN
      END
C-------------------------------------------------------------
```